On the Synthesis of Stable Walkover Gaits for the Acrobot

Emily Kao-Vukovich, Manfredi Maggiore

***Abstract*—We introduce a novel method of producing stable walking gaits for the acrobot using virtual holonomic constraints (VHCs). Using this method, we produce a new stable walking motion for the acrobot, the walkover gait. In this gait, the swing leg rotates counterclockwise up and over the stance leg, as opposed to the standard compass gait where the swing leg rotates clockwise and overlaps with the stance leg partway along the motion. The walkover gait is found by searching for a virtual holonomic constraint enjoying certain properties, among them the requirement of producing a stable hybrid limit cycle corresponding to walking. Key to the proposed approach is the recently developed notion of the virtual constraint generator (VCG), a control system on the configuration manifold of the robot whose solutions are all possible VHCs up to reparametrization. A systematic procedure is presented for the synthesis of VHCs achieving the desired walking motion for the acrobot, culminating in an optimal control problem for the VCG, solved numerically to produce the gait. Theoretical characterizations are given for the feasibility of the gait generation problem.**

I. Introduction

THIS paper investigates the problem of gait generation using virtual holonomic constraints (VHCs) for the walking acrobot depicted in Figure 1, an underactuated robot with two degrees-of-freedom and one actuator at the hip. The acrobot is the simplest bipedal robot, and there is a wealth of literature on designing acrobot gaits. In 1990, McGeer [1] discovered natural gaits for passive acrobots with rocker feet walking down an incline. This work spurred significant research in passive dynamic walking and passivity-mimicking controllers for actuated bipeds. In [2], Garcia et al. extended McGeer's work to show that a simpler passive acrobot model with point feet also exhibits stable gaits on shallow slopes. Goswami et al. designed controllers to track characteristics of passive gaits, such as average speed per step, to achieve stable walking for fully actuated acrobots on flat ground or even up shallow slopes [3]. Spong and collaborators took an energy-shaping approach. Their control design uses controlled symmetries to create a virtual gravitational force such that the acrobot behaves as though it is passively walking down some desired slope (see, e.g., [4], [5], [6]). Asano et al. took a similar approach in [7], taking into consideration stability of the zero moment-point. All of these control schemes require full actuation. However, bipedal robots are often underactuated, such as in the case of robots with point feet.

The authors are with the Department of Electrical and Computer Engineering, University of Toronto, Toronto, ON M5S 3G4, Canada (e-mail: emily.vukovich@mail.utoronto.ca, maggiore@control.utoronto.ca). This research was supported by the Natural Sciences and Engineering Research Council of Canada (NSERC).

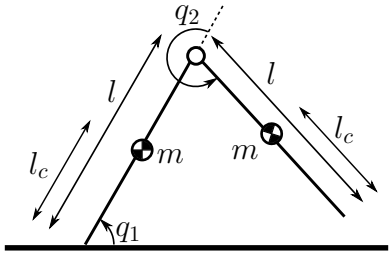

Fig. 1: The walking acrobot.

In the early 2000s, Grizzle and collaborators introduced the use of VHCs as a tool for bipedal motion control. This seminal work showed that for a system with one degree of underactuation, a judicious choice of virtual constraint will induce a stable hybrid limit cycle corresponding to a stable periodic gait (e.g., [8], [9], [10], [11], [12], [13]). In particular, the authors showed that enforcing a suitable virtual constraint condenses the stability analysis for the full-dimensional system down to a stability analysis for a two-dimensional system, from which one can extract conditions for the existence and stability of a stable hybrid limit cycle. The virtual constraint paradigm has been applied to numerous bipedal motion applications, such as bipedal robots (e.g., [14], [15], [16], [17], [18]), prosthetic legs (e.g., [19], [20]), and exoskeletons (e.g., [21]). Recent work has also extended this VHC theory to systems with higher degrees of underactuation, such as in [22] and [23].

The central challenge in the VHC approach is to design a constraint that not only achieves walking for one step, but also produces a stable hybrid limit cycle. The predominant approach is to express the virtual constraints using Bézier polynomials whose coefficients are determined through a nonlinear optimization procedure. Desired gait properties are posed as optimization constraints, and the cost is generally some measure of efficiency, such as the average sum squared torque over a step (e.g., [9], [12], [24]).

Contributions of this paper. This paper presents a novel gait synthesis method for the acrobot using virtual constraints. Similarly to the literature on bipedal locomotion cited above, we produce a desired walking motion by enforcing a virtual holonomic constraint (VHC) inducing a stable hybrid limit cycle. The novelty of the proposed approach is in the way in which the VHC is synthesized. We rely on the concept of the virtual constraint generator (VCG) recently developed by Otsason *et al.* in [25] to convert the gait synthesis problem into an optimal control problem for the VCG, which can then be

solved numerically to obtain a VHC inducing the desired gait. Our method allows for some degree of theoretical analysis of feasibility, something which is currently not present in the literature.

We introduce our novel method by way of a working example, the walkover gait. In this gait, one leg rotates counterclockwise up and over the other, as shown in Figure 2. The gait resembles the walkover manoeuvre in gymnastics, where the gymnast supports themselves on their hands and swings their legs up and over their head, landing in a backbend position. The walkover gait is an unusual gait that does not resemble natural biped motion, but it serves to demonstrate the types of complex motions that can be produced using the gait design technique proposed in this paper. There are three key specifications for walking.

First, the VHC curve must connect pre- and post-impact configurations of the robot, and this is a motion planning problem for the VCG. Proposition 1 in this paper gives necessary and sufficient conditions for the existence of a VHC solving the problem. In this context, we also want the curve to be contained in a safe set where the robot has no unwanted collisions with the ground, but we do not investigate this requirement theoretically.

Second, the VHC must satisfy the hybrid invariance conditions developed in [9] and avoid Zeno solutions in the constrained dynamics, and this translates to a requirement for the initial and final values of the control signal of the VCG producing the gait. In Proposition 2, we give necessary and sufficient conditions for the feasibility of this problem.

Finally, the VHC must induce a stable hybrid limit cycle, for which conditions were developed in [9]. These conditions impose a functional constraint on the trajectories of the VHC, which we formulate as an optimal control problem that also encompasses all other specifications. The numerical solution of this problem gives the desired gait. The technique presented here can be adapted to produce other gaits, for example compass gaits.

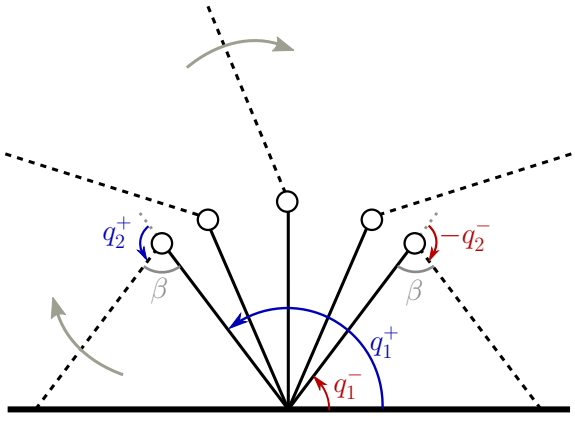

Fig. 2: The walkover gait.

Although the focus of this paper is on designing walkover gaits for the acrobot, with minimal modifications the proposed method can be used to generate different types gaits for the acrobot. Furthermore, several ideas and results are amenable to generalization to planar walking robots with degree of underactuation one, and we point this out at various points in the paper.

Comparison to existing literature. The gait synthesis method presented in this paper follows directly from the hybrid zero dynamics (HZD) theory of Grizzle et al. in [26]. Our method of gait synthesis, however, differs fundamentally from that of [26]. Virtual constraints must satisfy a regularity condition whereby, viewed as outputs of the robot, they yield a well-defined relative degree of two. The approach of [26] involves searching over the space of all Bézier curves of a specified degree (e.g., [9], [12], [23]) and imposing regularity as a constraint in the optimization process. The method proposed in this paper has the regularity requirement built-in: all solutions of the VCG are automatically regular VHCs. Existing HZD methods rely on an a priori parametrization of the VHCs which restricts the class of constraints that these methods can produce. Among other things, the designer is required to choose a so-called timing variable for the VHC which must be monotonic along closed-loop solutions satisfying the constraint. In contrast, the optimal control formulation proposed in this paper searches the space of *all* regular VHCs and does not require the designer to choose a timing variable.

Another difference with existing HZD methods is that the approach proposed here is amenable to theoretical analysis. For example, one can ask questions such as "Does there exist a VHC connecting two configurations and guaranteeing hybrid invariance?". These questions can be converted to control-theoretic questions for the VCG, and insight can be derived from their investigation. For instance, in this paper we find that only certain leg apertures (the angle β in Figure 2) are compatible with walking motion. We provide a more detailed comparison between our approach and other HZD methods in Section XI.

In this paper we are concerned with producing a walkover gait for the acrobot. To the best of our knowledge, the walkover gait has not yet been proposed for the acrobot using virtual constraints. A motion similar to the walkover gait is investigated in [27] for an acrobot with rounded links. This work features a similar backbending motion, however due to the curved links the acrobot exhibits a rolling motion and so never impacts the ground. Further, our method can be used to produce stable walkover gaits where the acrobot walks uphill for very shallow inclines. The walkover gait is reminiscent of the underhand brachiating gait (e.g., [28], [29], [30]), but with the effect of gravity reversed. The problems of the brachiating gait and the walkover gait also differ in that the brachiating gait is designed to reduce velocity as the swing arm approaches the ceiling in order to minimize the effect of collisions with the ceiling [29], [30]. In contrast, since the acrobot is walking on the ground, we allow for collisions and instead the approach in this paper follows the method of Grizzle and collaborators, and uses a model of the impacts.

The work of Asano in [31] shares some similarities with this paper. Asano finds virtual constraints as the solution to a boundary value problem for a set of differential equations in a modified phase variable. In this paper we also pose the constraint design problem as the solution to a boundary value

problem, however our approach operates in the configuration space. Furthermore, Asano's approach is designed to handle gaits where the stride length changes from step to step, and so does not require that the constraint correspond to a stable hybrid limit cycle. Finally, Asano's approach requires that the acrobot legs are bent to shift their centres of mass in the direction of the gait. In this paper we consider the case of completely straight legs.

Paper organization. In Section II we formulate the walkover gait generation problem. In Sections III and IV we present the hybrid model of walking for the acrobot and concisely review the preliminary notions needed for subsequent development. In Section V we outline our strategy for gait generation. In Sections VI and VII we characterize the existence of VHC curves connecting two points in the configuration manifold and enjoying the hybrid invariance property. In Section VIII we formulate an optimal control problem for gait synthesis, and in Section IX we present simulation results. In Section X, we discuss practical aspects of controller implementation, in particular ways to take into account ground reaction forces at impact. We also discuss the generalizability of our results. In Section XI, we compare the procedures of this paper to those presented in [12] as well as the more recent techniques in FROST, a state-of-the-art toolbox for generating VHCs. Concluding remarks are made in Section XII.

Notation. We denote by $\mathbb{S}^1$ the unit circle in $\mathbb{R}^2$. If $h : \mathbb{R}^n \to \mathbb{R}^m$ is a smooth function, and $q \in \mathbb{R}^n$ we denote by dh_q the Jacobian matrix of h at q. If $\mathcal{Q}$ is a smooth manifold and $p \in \mathcal{Q}$, then we denote the tangent space to $\mathcal{Q}$ at p by $T_p\mathcal{Q}$ and the tangent bundle of $\mathcal{Q}$ by $T\mathcal{Q}$. If f is a vector field on $\mathbb{R}^n$ and $q \in \mathbb{R}^n$ then $\mathcal{O}^f(q)$ denotes the orbit of f through q, and $\Phi_t^f(q)$ denotes the flow of f from q at time t. We use the shorthand notation s_q for $\sin(q)$ and c_q for $\cos(q)$. For a positive integer n, we denote by I_n the $n \times n$ identity matrix. We denote by $\|v\|$ the Euclidean norm of a vector $v \in \mathbb{R}^2$, and by $\langle v, w \rangle$ the Euclidean inner product of vectors $v, w \in \mathbb{R}^2$.

II. Problem formulation

In this paper we generate stable walking gaits for the acrobot producing the kind of walkover motion depicted in Figure 2. This motion describes a "backbending" behaviour, where one leg swings clockwise and over the other, in contrast with the traditional compass gait where one leg swings counterclockwise and in front of the other. We assume that the two legs are identical. We further assume that the stance foot is pinned to the ground during the stance phase.[1]

The configuration variables of the acrobot are the angle q_1 of its stance leg with the ground, and the relative angle q_2 between the two legs, as illustrated in Figure 1. When defining the walkover gait, we need to account for the direction and number of revolutions performed by the legs. For this reason, we consider the angles q_1 and q_2 as elements of $\mathbb{R}$, and we take the configuration manifold of the pinned acrobot to be $\mathcal{Q} = \mathbb{R}^2$, and its state space to be $T\mathcal{Q} = \mathbb{R}^2 \times \mathbb{R}^2$.

[1]In practice, this could be achieved via a mechanism, e.g., an electropermanent magnet, which locks the stance foot in place during the swing phase and releases the stance foot when the swing foot impacts the ground. This assumption is essential as it allows us to disregard requirements on ground reaction forces. Inclusion of ground reaction forces as optimization constraints is the subject of future research, as discussed in Section X.

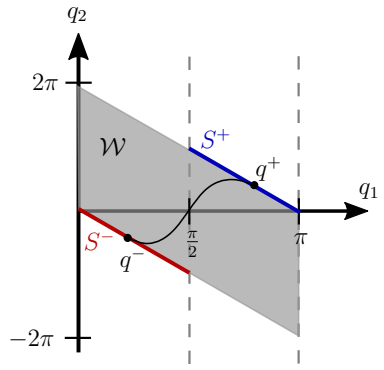

Fig. 3: Impact surfaces and safe set for walkover gait.

Impact with the ground occurs whenever the tip of the swing leg hits the ground, and one can easily see that this happens whenever the configuration vector q is on the **pre-impact surface** $S^- \subset \mathcal{Q}$, defined as

$$S^- := \{(q_1, q_2) \in [0, \pi/2] \times \mathbb{R} : q_2 = -2q_1\}. \quad (1)$$

Note the restriction $q_1 \in [0, \pi/2]$ reflecting the fact that for an appropriately designed walking gait, the swing leg impacts the ground ahead of the stance leg. We denote by $q^- \in S^-$ the configuration vector when the swing leg hits the ground.

Immediately after impact, the two legs swap identity, resulting in a relabelling of the configuration variables. Letting $R : \mathcal{Q} \to \mathcal{Q}$ be the function mapping q to its relabelled counterpart (this function is presented in Section III), the pre-impact surface gets mapped via R to the **post-impact surface**

$$S^+ = \{(q_1, q_2) \in [\pi/2, \pi] \times \mathbb{R} : q_2 = -2q_1 + 2\pi\}. \quad (2)$$

The pre- and post-impact surfaces are depicted in Figure 3. We let $q^+ := R(q^-) \in S^+$ denote the relabelled configuration vector at impact. In describing the gait, we take the convention that the gait starts at the post-impact state $q^+ \in S^+$ and ends at the pre-impact state $q^- \in S^-$, just as depicted in Figure 2.

A symmetric gait requires that the acrobot begin and end a step with the same leg aperture, denoted β (see Figure 2). A choice of β uniquely characterizes q^+ and q^- as follows:

$$q^+ := \begin{bmatrix} \frac{\beta+\pi}{2} \\ \pi - \beta \end{bmatrix}, \quad q^- := \begin{bmatrix} \frac{\pi-\beta}{2} \\ \beta - \pi \end{bmatrix}. \quad (3)$$

The walkover gait will make the robot's configuration transition between $q^+ \in S^+$ and $q^- \in S^-$ with the further constraint that the configuration q be contained in the **safe set**

$$\mathcal{W} = \{(q_1, q_2) : 0 \le q_1 \le \pi, -2q_1 \le q_2 \le 2\pi - 2q_1\}, \quad (4)$$

so that the stance leg remains above-ground (i.e., $0 < q_1 < \pi$) and the swing leg stays within one counter-clockwise revolution of the stance leg (i.e., $-2q_1 < q_2 < 2\pi - 2q_1$).

In this paper, as in much literature on bipedal locomotion, a gait will be described by a parametric curve $q = \sigma(\theta)$

representing a virtual holonomic constraint (VHC) that will be stabilized via feedback control. Designing a gait means designing a VHC curve that connects $q^+ \in S^+$ to $q^- \in S^-$ and is entirely contained in the safe set $\mathcal{W}$. VHCs are reviewed in Section IV-A.

In addition to being contained in the safe set $\mathcal{W}$, to ensure that there are well-defined constrained dynamics in the presence of impacts, the curve $q = \sigma(\theta)$ must have unique intersections with S^+ and S^- and meet the so-called hybrid invariance conditions presented in [9]. Additionally, we also want the constrained dynamics to have no Zeno solutions, i.e., solutions where the state jumps indefinitely and time does not progress. These notions are reviewed in Section IV-B.

Finally, the VHC curve must give rise to constrained dynamics with an asymptotically stable hybrid limit cycle. These conditions were developed in [9] (see also [12]) and are reviewed in Section IV-B. The foregoing considerations are summarized in the next problem statement.

Gait Generation Problem. *Given a fixed impacting aperture β, find a regular* VHC *curve $\sigma : \mathbb{R} \to Q$ for the acrobot meeting the following specifications (see Figure 3):*

G.A Walkover motion: *there exist θ_a, $\theta_b \in \mathbb{R}$, $\theta_a < \theta_b$, such that*

$$\begin{cases} \sigma(\theta_a) = q^+ \\ \sigma(\theta_b) = q^- \\ \sigma(\theta) \in \mathcal{W} \qquad \theta \in (\theta_a, \theta_b), \end{cases} \tag{5}$$

with q^+ and q^- given in (3)*.*

G.B Hybrid invariance*: the constraint manifold Γ induced by the* VHC *curve $q = \sigma(\theta)$ satisfies the hybrid invariance condition C1 reviewed in Section IV-B. Moreover, the hybrid constrained dynamics do not have Zeno solutions.*

G.C Stable hybrid limit cycle: *the* VHC *curve $q = \sigma(\theta)$ induces constrained dynamics with an asymptotically stable hybrid limit cycle (see conditions in* (19) *of Section IV-C).*

We remark that the requirement of a unique intersection of the VHC with S^+, S^- is built into specification G.A.

III. Walking acrobot model

In this section we present the hybrid model of walking for the acrobot of Figure 1. Each leg has length l, mass m, and centre of mass at distance l_c from the point foot, as shown in Figure 1. We denote by I_z the moment of inertia of each leg at its centre of mass. In modelling this robot and its impacts with the ground, we follow the methodology presented in [12].

Swing Phase Model. During the swing phase, we assume that the stance foot is pinned to the ground and as such the dynamics are described by

$$D(q)\ddot{q} + C(q,\dot{q})\dot{q} + \nabla P(q) = B\tau, \tag{6}$$

where $q = [q_1 \quad q_2]^\top$ are the generalized coordinates as shown in Figure 1, and

$$D(q) = \begin{bmatrix} m(2l_c^2 + l^2 + 2ll_c c_{q_2}) + 2I_z & m(l_c^2 + ll_c c_{q_2}) + I_z \\ m(l_c^2 + ll_c c_{q_2}) + I_z & ml_c^2 + I_z \end{bmatrix}, \tag{7}$$

$$C(q,\dot{q}) = -mll_c s_{q_2} \begin{bmatrix} \dot{q}_2 & \dot{q}_1 + \dot{q}_2 \\ -\dot{q}_1 & 0 \end{bmatrix},$$

$$P(q) = Gs_{q_1}(ml_c + ml) + Gs_{q_1+q_2} ml_c.$$

The matrix B is given by $B = [0 \quad 1]^\top$ as the acrobot is actuated at the hip, and so the acrobot model has two degrees of freedom and one actuator, $\tau \in \mathbb{R}$. The state of this system is $x = [q^\top \quad \dot{q}^\top]^\top \in T\mathcal{Q}$. In what follows, let $p^v(q)$ denote the height of the swing foot from the ground, given by $p^v(q) = l(s_{q_1} + s_{q_1+q_2})$.

Hybrid model of walking. The model of the walking acrobot is a hybrid dynamical system

$$\begin{cases} D(q)\ddot{q} + C(q,\dot{q})\dot{q} + \nabla P(q) = B\tau & (q,\dot{q}) \in \mathsf{C} \\ (q^+,\dot{q}^+) = \Delta(q^-,\dot{q}^-) & (q,\dot{q}) \in \mathsf{D}, \end{cases} \tag{8}$$

whereby the swing phase model (6) is augmented with a so-called **impact map** Δ making the state jump whenever the tip of the swing leg hits the ground. The flow and jump sets, C and D, are defined as

$$\mathsf{C} = \{(q,\dot{q}) \in T\mathcal{Q} : q_1 \in [0,\pi], p^v(q) \geq 0\}$$
$$\mathsf{D} = \{(q,\dot{q}) \in T\mathcal{Q} : q_1 \in [0,\pi], p^v(q) \leq 0\}.$$

The restriction $q_1 \in [0,\pi]$ is made so that the stance leg remains above the ground. The impact map reflects the fact that when the swing foot impacts the ground, it becomes pinned to the ground, the stance leg is released, and the identities of the legs are swapped. Since the flow and impact maps are smooth, and since the flow and jump sets C, D are closed, this hybrid dynamical system satisfies the hybrid basic conditions of [32], and is therefore well-posed.

In this paper we use the impact map and related assumptions presented in [12]. In particular, we assume that at impact the ground reaction forces are impulsive and there is no instantaneous change in configuration. As in [12], we break down the derivation of the impact map into three phases:

Pre-impact phase with state $(q^-,\dot{q}^-)$. The tip of the swing leg has reached the ground. This occurs when $q(t)$ hits the pre-impact surface S^- defined in (1).

Post-impact phase with state $(q^0,\dot{q}^0)$. The impulsive ground reaction forces have caused the generalized velocity $\dot{q}$ to jump from $\dot{q}^-$ to $\dot{q}^0$, while $q^0 = q^-$ because the impact does not cause the angles to change. We seek to find the map $\Delta_1 : S^- \times \mathbb{R}^2 \to S^- \times \mathbb{R}^2$, $(q^-,\dot{q}^-) \mapsto (q^0,\dot{q}^0)$.

Following [12], Δ_1 is derived by first unpinning the stance foot at the moment of impact. Integrating the equations of motion over the impulsive impact event, one obtains an equation for the variation of generalized momentum at impact. Finally, by imposing the conditions of no slip and no rebound

of the swing foot at impact and solving for the relation between $\dot{q}^0$ and $\dot{q}^-$, ones arrives at the relation $\dot{q}^0 = \Omega(q^-)\dot{q}^-$, where

$$\Omega(q^-) = \begin{bmatrix} I_2 & 0_{2\times 2} \end{bmatrix} \left[I_4 - D_e^{-1} E^\top (E D_e^{-1} E^\top)^{-1} E \right] \begin{bmatrix} I_2 \\ 0_{2\times 2} \end{bmatrix} \tag{9}$$

and the matrix-valued functions D_e and E, given in Appendix A, are evaluated at q^-. In conclusion, the map Δ_1 is given by $\Delta_1(q^-, \dot{q}^-) = \big(q^-, \Omega(q^-)\dot{q}^-\big)$.

Relabelling phase with state $(q^+, \dot{q}^+)$. The identities of the legs are swapped, and as a result the state of the acrobot is relabelled. We seek to find the map $\Delta_2 : S^- \times \mathbb{R}^2 \to S^+ \times \mathbb{R}^2$, $(q^0, \dot{q}^0) \mapsto (q^+, \dot{q}^+)$. Figure 4 illustrates the relationship between q^0 and q^+, and it is easily seen that

$$q^+ = R(q^0) = -q^0 + \begin{bmatrix} \pi \\ 0 \end{bmatrix}. \tag{10}$$

One can easily see that the post-impact surface presented in (2) is given by $S^+ = R(S^-)$. The map $\Delta_2 : S^- \times \mathbb{R}^2 \to S^+ \times \mathbb{R}^2$, $(q^0, \dot{q}^0) \mapsto (q^+, \dot{q}^+)$ is given by

$$\Delta_2(q^0, \dot{q}^0) = \big(R(q^0), dR_{q^0}\dot{q}^0\big) = \big(-q^0 + [\pi \ 0]^\top, -\dot{q}^0\big).$$

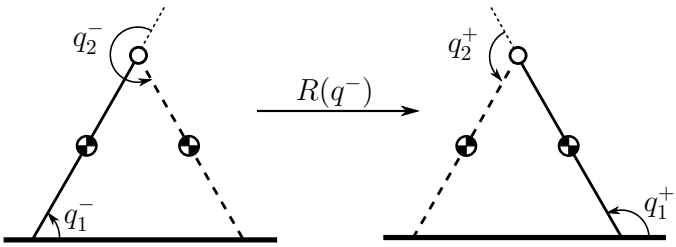

Fig. 4: Effect of relabelling map on acrobot configuration variables. The solid line represents the stance leg and the dashed line represents the swing leg.

Impact model: The impact map Δ is the composition of Δ_1 and Δ_2, $\Delta := \Delta_2 \circ \Delta_1 : S^- \times \mathbb{R}^2 \to S^+ \times \mathbb{R}^2$, and it maps the pre-impact state $(q^-, \dot{q}^-)$ to the post-impact, relabelled state $(q^+, \dot{q}^+)$ as follows:

$$\Delta(q^-, \dot{q}^-) = \big(R(q^-), -\Omega(q^-)\dot{q}^-\big), \tag{11}$$

with $\Omega(q^-)$ and $R(q^-)$ given in (9) and (10), respectively. This concludes the derivation of the hybrid model of walking (8).

IV. Preliminary notions

In this section we briefly review virtual holonomic constraints focusing on the two DOFs system (6) and its hybrid counterpart (8). We also recall the hybrid reduced dynamics induced by a VHC and the conditions for the existence of a stable hybrid limit cycle originally presented in [9] (see also the book [12]). The general theory can be found in [33], [34], [9].

A. Virtual constraints and constrained dynamics

A regular **virtual holonomic constraint** (VHC) for the mechanical system without impacts (6) is an embedded curve $\mathcal{C}$ in the configuration manifold $\mathcal{Q}$ satisfying the transversality condition

$$(\forall q \in \mathcal{C}) \ T_q\mathcal{C} \oplus \mathrm{Im}(D^{-1}(q)B) = T_q\mathcal{Q}. \tag{12}$$

Geometrically, the condition requires that the control input τ imparts accelerations in a direction transversal to $\mathcal{C}$.

If the curve $\mathcal{C}$ is expressed *implicitly* as a relation $\mathcal{C} = \{q \in \mathcal{Q} : h(q) = 0\}$, where $h : \mathcal{Q} \to \mathbb{R}$ is C^2 and has nonvanishing Jacobian on $\mathcal{C}$, then the transversality condition (12) amounts to requiring system (6) with output $e = h(q)$ to have a well-defined relative degree 2 on $\mathcal{C}$. The zero dynamics manifold ([35]),

$$\Gamma := \{(q, \dot{q}) \in T\mathcal{Q} : h(q) = 0, \ dh_q\dot{q} = 0\},$$

is called the **constraint manifold** associated with the VHC $h(q) = 0$, and it is the set where the constraint $h(q) = 0$ is satisfied and the velocities $\dot{q}$ are tangent to $\mathcal{C}$. From a dynamical viewpoint, Γ is the largest subset of $T\mathcal{Q}$ that can be made invariant via feedback control and such that solutions $(q(t), \dot{q}(t))$ satisfy $h(q(t)) \equiv 0$. Taking two derivatives of the output e along solutions of (6), one obtains an expression of the form $\ddot{e} = F(q, \dot{q}) + (dh_q D^{-1} B)\tau$, and since the output $e = h(q)$ yields relative degree 2, the coefficient $dh_q D^{-1}(q)B$ is nonzero on $\mathcal{C}$. The smooth feedback linearizing controller

$$\tau^\star(q, \dot{q}) = (dh_q D^{-1} B)^{-1}(-K_p h(q) - K_d dh_q \dot{q} - F(q, \dot{q}))$$

locally asymptotically stabilizes[2] Γ.

One may also express the VHC curve $\mathcal{C}$ *parametrically* as $\mathcal{C} = \{q \in \mathcal{Q} : q = \sigma(\theta), \theta \in \mathbb{R}\}$, where σ is C^2 and has nonvanishing derivative, in which case we speak of a **parametric VHC**, and the transversality condition (12) becomes

$$(\forall \theta \in \mathbb{R}) \ \mathrm{span}\{\sigma'(\theta)\} \oplus \mathrm{Im}(D^{-1}(q)B)\Big|_{q=\sigma(\theta)} = T_{\sigma(\theta)}\mathcal{Q}. \tag{13}$$

The variable $\theta \in \mathbb{R}$ parametrizing the VHC curve is called the **phase variable** of the constraint. With this parametrization, the constraint manifold is given by $\Gamma = \{(q, \dot{q}) \in T\mathcal{Q} : q = \sigma(\theta), \ \dot{q} = \sigma'(\theta)\dot{\theta}, \ \theta, \dot{\theta} \in \mathbb{R}\}$ and, if the curve is open, the map $\Sigma : (\theta, \dot{\theta}) \in \mathbb{R} \times \mathbb{R} \mapsto (\sigma(\theta), \sigma'(\theta)\dot{\theta}) \in T\mathcal{Q}$ is an embedding and its image is Γ.

The parametric description of a VHC allows us to express the system dynamics on the constraint manifold in terms of only the phase variable θ and its derivative, $\dot{\theta}$. Substituting $(q, \dot{q}) = \Sigma(\theta, \dot{\theta})$ in (6) and premultiplying both sides of the equation by a rank 1 left-annihilator of B, $B^\perp = [-1 \quad 0]$, we get the **constrained dynamics**

$$\ddot{\theta} = \Psi_1(\theta) + \Psi_2(\theta)\dot{\theta}^2, \tag{14}$$

[2]There is an additional requirement for the stabilizability of VHCs, presented in [33].

where

$$\Psi_1(\theta) = -\frac{B^\perp \nabla P}{B^\perp D\sigma'}\Big|_{q=\sigma(\theta)}, \tag{15a}$$

$$\Psi_2(\theta) = -\frac{1}{B^\perp D\sigma'}\left[B^\perp(D\sigma'' + C(\sigma,\sigma')\sigma')\right]\Big|_{q=\sigma(\theta)}. \tag{15b}$$

The reason why (14) is called the constrained dynamics is this: if Γ is rendered invariant by a feedback controller, then all solutions of the closed-loop system on Γ have the form $(q(t), \dot{q}(t)) = \Sigma(\theta(t), \dot{\theta}(t))$, where $\theta(t)$ is a solution of (14).

It was shown in [36] that if $\mathcal{C}$ is an open curve (as it is for any walking acrobot gait), then the reduced dynamics are Euler-Lagrange, with Lagrangian $\mathcal{L} = \frac{1}{2}M(\theta)\dot{\theta}^2 - V(\theta)$, where M and V are the virtual mass and virtual potential, defined as:

$$M(\theta) = \exp\left\{-2\int_{\theta_a}^{\theta}\Psi_2(\xi)d\xi\right\}, \tag{16a}$$

$$V(\theta) = -\int_{\theta_a}^{\theta}\Psi_1(\xi)M(\xi)d\xi, \tag{16b}$$

where θ_a is an arbitrary fixed parameter. In Section IV-B, θ_a will represent the value of the phase variable associated with the beginning of a step.

B. Hybrid constrained dynamics

We now consider virtual constraints in the context of the hybrid dynamical system (8). Following [9], [12], we seek a VHC $\mathcal{C}$ satisfying these two conditions:

- C1 **Hybrid Invariance of Γ:** if $q \in \mathcal{C} \cap S^-$ and $\dot{q} \in T_q\mathcal{C}$, then $\Delta(q,\dot{q}) \in T_q\mathcal{C}$. That is, if the acrobot impacts the ground while on the constraint manifold, the impact map keeps the state on the constraint manifold.
- C2 **Unique Intersection:** $\mathcal{C} \cap S^-$ must be a unique point. Let q^- be this point of intersection. Then there is a unique θ_b such that $\sigma(\theta_b) = q^-$.

Under these two assumptions, following the development in [12], there is a reduced impact map on Γ represented using $(\theta, \dot{\theta})$ coordinates. Using the parameterization $q = \sigma(\theta)$, we obtain the effect of the relabelling map on θ,

$$\theta_a = \sigma^{-1}(R(\sigma(\theta_b))).$$

The jump in velocities is given by $\dot{q}^+ = -\Omega(q^-)\dot{q}^-$. Writing this in terms of θ and solving for $\dot{\theta}_a$, we obtain $\dot{\theta}_a = \delta\dot{\theta}_b$, where

$$\delta = -\frac{\langle \sigma'(\theta_a), \Omega(q^-)\sigma'(\theta_b)\rangle}{\|\sigma'(\theta_a)\|^2}. \tag{17}$$

Note that $\delta \neq 0$ since $\dot{q}^+ = \sigma'(\theta_a)\dot{\theta}_a \neq 0$ by the assumption that the stance leg detaches from the ground on impact. Recalling the definition of the flow set C in Section III, we assume without loss of generality that $\theta_a < \theta_b$ and that $\sigma(\theta) \in \mathsf{C}$ if and only if $\theta \in [\theta_a, \theta_b]$. Then the flow set of the constrained dynamics is $\hat{\mathsf{C}} = [\theta_a, \theta_b] \times \mathbb{R}$, and the jump set is $\hat{\mathsf{D}} = \big((-\infty, \theta_a] \cup [\theta_b, \infty)\big) \times \mathbb{R}$.

In conclusion, if $q = \sigma(\theta)$ is a parametric VHC satisfying conditions C1 and C2 then the dynamics on the constraint manifold Γ are described by the hybrid dynamical system:

$$\begin{cases} \ddot{\theta} = \Psi_1(\theta) + \Psi_2(\theta)\dot{\theta}^2 & (\theta,\dot{\theta}) \in \hat{\mathsf{C}} \\ (\theta,\dot{\theta})^+ = (\theta_a, \delta\dot{\theta}) & (\theta,\dot{\theta}) \in \hat{\mathsf{D}}. \end{cases} \tag{18}$$

The reduced impact map is the second equation in (18). We remark that if $\delta < 0$, all solutions $(\theta(t), \dot{\theta}(t))$ of (18) reaching the line $\{(\theta,\dot{\theta}) : \theta = \theta_b\}$ stop flowing and jump indefinitely, causing Zeno behaviour. The requirement $\delta > 0$ will be built in the design of our VHC, see Section VII.

C. Stable hybrid limit cycles

The work in [9], [12] presents the following conditions for existence and stability of hybrid limit cycles in the constrained dynamics[3]:

$$0 < \frac{\delta^2}{M(\theta_b)} < 1, \tag{19a}$$

$$\frac{V(\theta_b)\delta^2}{M(\theta_b) - \delta^2} + V_{\max} < 0, \tag{19b}$$

where $V_{\max} := \max_{\theta\in[\theta_a,\theta_b]} V(\theta)$. The analysis in [12] is of Poincaré type. The authors choose the Poincaré section $\{(\theta,\dot{\theta}) : \theta = \theta_b\}$, and show that, under the conditions (19), there is a fixed point in the section, and the eigenvalue of the linearization of the Poincaré map at this fixed point is $\delta^2/M(\theta_b)$. We will make use of the eigenvalue $\delta^2/M(\theta_b)$ in Section IX.

V. Basic idea for gait generation

We have seen in Section II that the gait generation problem involves finding a parametric VHC $q = \sigma(\theta)$ contained in the safe set $\mathcal{W} \subset \mathcal{Q}$ and connecting two points q^+ and q^- uniquely determined by the leg aperture β as per (3). This curve must also meet specifications G.B, G.C. One could follow the approach in, e.g., [12], [23], and let $\sigma(\theta)$ be a set of Bézier polynomials, then formulate a constrained parameter optimization problem for these polynomials. The constraints of this program would be the identities $\sigma(\theta_a) = q^+$, $\sigma(\theta_b) = q^-$, the containment in $\mathcal{W}$, the regularity property in (13), and specifications G.B, G.C. While this approach will be successful in a number of practical scenarios, it is not amenable to theoretical analysis. Existential questions such as "Does there exist a VHC curve connecting q^+ and q^-?" cannot be easily formulated in this setup, and one is unlikely to gain much theoretical insight on a given problem. To illustrate, a byproduct of the development of this paper is that the gait generation problem is *unsolvable* for certain values of the leg aperture β, and there are precise conditions ensuring the existence of a VHC curve connecting two points. Another consideration is that the parametric space of Bézier

[3]Note that in [12], the authors express equations (19) and the eigenvalue of the linearized Poincaré map using a different set of coordinates; the detailed derivation of these conditions using the $(\theta,\dot{\theta})$ coordinates of system (18) is found in [37].

polynomials can be large, and it would be desirable to restrict the search to just the space of all regular VHC curves.

Let $f_{\text{acr}} := (B^{\perp})^{\top} = \begin{bmatrix} -1 & 0 \end{bmatrix}^{\top}$ and $g_{\text{acr}}(q) := D^{-1}(q)B$, and consider the single-input planar control system

$$\frac{dq}{d\theta} = f_{\text{acr}}(q) + g_{\text{acr}}(q)u. \tag{20}$$

For each $q \in \mathcal{Q}$ and $u \in \mathbb{R}$, the vector $f_{\text{acr}}(q) + g_{\text{acr}}(q)u$ is transversal to the subspace $\text{Im}(D^{-1}(q)B)$, and therefore any solution $q = \sigma(\theta)$ of the differential equation (20) for arbitrary C^1 control signal $u(\theta)$ satisfies the transversality condition (13). One expects, therefore, that all solution curves of (20) should be parametric VHCs for system (6), and in fact we have an even stronger result. In [25] it was shown that if $q = \sigma(\theta)$ is a parametric VHC for system (6), then up to reparametrization, $\sigma(\theta)$ is a solution of the control system (20). Vice versa, if $q = \sigma(\theta)$ is a solution of (20) for a C^1 control signal $u : \mathbb{R} \to \mathbb{R}$, and if it is an embedded curve, then it is a parametric VHC for system (6). In short, the set of embedded solutions of (20) for C^1 control signals coincides, up to reparametrization, with the set of *all* parametric VHCs, and for this reason (20) is called the **virtual constraint generator (VCG)** of system (6). The control input u of the VCG will be referred to as the **virtual control**.

We now outline our strategy for addressing each of the subproblems G.A through G.C. We we explore each subproblem in detail in Sections VI, VII, and VIII. Searching for a gait, i.e., a parametric VHC connecting two points q^+ and q^- in $\mathcal{Q}$, corresponds to setting $q(0) = q^+$, and finding a C^1 virtual control signal $u(\theta)$ producing a solution of (20) that reaches[4] q^- in finite time θ. Thus specification G.A is a motion planning problem for the VCG (20). In Section VI we investigate conditions for the existence of a solution to this problem. As we shall see in Section VII, enforcing the hybrid invariance requirement G.B amounts to restricting the initial and final values of the virtual control signal $u(\theta)$. Finally, the requirement G.C that the VHC induces a stable hybrid limit cycle amounts to two functional constraints on the solutions of the VCG (20). The above considerations will lead to the formulation of an optimal control problem for the VCG (20), the solution to which will be a gait solving the gait generation problem. To summarize, these are the next steps of our development:

1) **Motion planning** (Section VI): Find conditions under which two points $q^+, q^- \in \mathcal{Q}$ can be connected by a solution of (20).
2) **Hybrid invariance** (Section VII): Find requirements on the initial and final values of virtual control inputs for the VCG (20) to guarantee hybrid invariance of the constraints it generates.
3) **Optimal control formulation** (Section VIII): Frame the gait generation problem as an optimal control problem for the VCG (20), and numerically determine the optimal virtual control signal for the VCG.

[4]Since the orientation of the solution curve of (20) is immaterial for the purpose of determining parametric VHCs, we simultaneously consider the complementary problem of setting $q(0) = q^-$ and seeking to reach q^+.

We remark that although the focus of this paper is on the design of walking gaits for the acrobot, some aspects of the discussion above are of a general nature. In particular, the observation made earlier that the design of a VHC curve connecting two points is mathematically equivalent to a motion planning problem for the VCG is true for any mechanical system with degree of underactuation one.

VI. Point to Point Motion Planning

In this section we investigate this motion planning problem: find conditions for the existence of a piecewise continuous virtual control signal $u(\theta)$ for the VCG (20) such that the corresponding solution $\sigma(\theta)$ of (20) satisfies $\sigma(\theta_a) = q^+$ and $\sigma(\theta_b) = q^-$, for some $\theta_a, \theta_b \in \mathbb{R}$. Since we do not care about the orientation of VHC curves, we do not require that $\theta_a < \theta_b$. For $q^0 \in \mathcal{Q}$, we denote by $\mathcal{R}(q^0)$ the set of states reachable set from q^0 in positive time by solutions of (20). The problem above can be restated as follows. Given $q^+, q^- \in \mathbb{R}^2$, find conditions under which either $q^- \in \mathcal{R}(q^+)$ or $q^+ \in \mathcal{R}(q^-)$. For convenience, we will refer to this problem as MP.

Generally, the characterization of reachable sets of nonlinear control systems is hard, but in the case of the VCG (20), a control affine system on the plane in which the drift and control vector fields are everywhere linearly independent, such characterization can be carried out to a satisfactory conclusion. Indeed, for control systems such as (20), [38, Theorem 2.1] states that for each $q^0 \in \mathcal{Q}$, the boundary $\partial\mathcal{R}(q^0)$ is the union of orbits of g_{acr}. Since $\|g_{\text{acr}}\|$ is bounded away from zero on $\mathcal{Q}$, all orbits of g_{acr} are embedded curves in $\mathcal{Q}$, and therefore they are diffeomorphic to either $\mathbb{R}$ or $\mathbb{S}^1$. Since g_{acr} has no equilibria, the Poincaré-Bendixson theorem implies that the orbits of g_{acr} are diffeomorphic to $\mathbb{R}$. Being embedded in $\mathcal{Q}$, each orbit $\mathcal{O}^{g_{\text{acr}}}(q^0)$ of g_{acr} divides $\mathbb{R}^2$ into two disjoint open subsets, as shown in Figure 5. Denoting these two subsets $\mathcal{D}^+(q^0)$ and $\mathcal{D}^-(q^0)$, with the convention that $f(q^0)$ points to the interior of $\mathcal{D}^+(q^0)$, we have

$$\mathcal{D}^+(q^0) \cup \mathcal{O}^{f_{\text{acr}}}(q^0) \cup \mathcal{D}^-(q^0) = \mathbb{R}^2 \text{ (disjoint union)}.$$

We remark that the set $\mathcal{D}^+(q^0)$ is positively invariant for (20) under any choice of control signal.

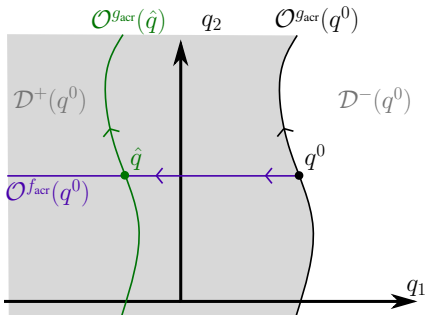

Fig. 5: Example of an integral curve $\mathcal{O}^{g_{\text{acr}}}(\hat{q})$ that is reachable from q^0. All points to the left of $\mathcal{O}^{g_{\text{acr}}}(q^0)$ are reachable in positive time.

For each $t > 0$, letting $\hat{q} = \Phi_t^{f_{\text{acr}}}(q^0)$, we have that $\hat{q} \in \mathcal{R}(q^0)$, and therefore $\mathcal{O}^{g_{\text{acr}}}(\hat{q}) \cap \mathcal{R}(q^0) \neq \emptyset$. Since $\mathcal{R}(q^0)$ is an open set, this latter conclusion implies, in light of [38,

Theorem 2.1], that $\mathcal{O}^{g_{\text{acr}}}(\hat{q}) \cap \partial\mathcal{R}(q^0) = \emptyset$. Together, the properties $\mathcal{O}^{g_{\text{acr}}}(\hat{q}) \cap \mathcal{R}(q^0) \neq \emptyset$ and $\mathcal{O}^{g_{\text{acr}}}(\hat{q}) \cap \partial\mathcal{R}(q^0) = \emptyset$ imply that $\mathcal{O}^{g_{\text{acr}}}(\hat{q}) \subset \mathcal{R}(q^0)$. Since $\hat{q} \neq q^0$ is an arbitrary point on the positive semiorbit $\mathcal{O}^{f_{\text{acr}}}(q^0)$, we have

$$\bigcup_{\hat{q}=\Phi_t^f(q^0),t>0} \mathcal{O}^{g_{\text{acr}}}(\hat{q}) \subset \mathcal{R}(q^0).$$

Now note that f_{acr} is a constant vector field whose orbits are straight horizontal lines, and the orbits of g_{acr} are parallel translations of the orbit $\mathcal{O}^{g_{\text{acr}}}(q^0)$ displayed in Figure 5. It follows that, for each $q^0 \in \mathcal{Q}$, the orbit of f_{acr} through q^0 crosses all orbits of g_{acr} in $\mathcal{D}^+$ in positive time, and therefore the set on the left-hand side of the above inclusion is the entire $\mathcal{D}^+(q^0)$. This establishes that $\mathcal{D}^+(q^0) \subset \mathcal{R}(q^0)$. Since $\mathcal{D}^+(q^0)$ is positively invariant for (20) under any control signal, we also have $\mathcal{R}(q^0) \subset \mathcal{D}^+(q^0)$, and we reach the conclusion that

$$\mathcal{D}^+(q^0) = \mathcal{R}(q^0).$$

We have thus reached a full characterization of the reachable set $\mathcal{R}(q^0)$ for the VCG (20). We now return to our motion planning problem MP: find conditions under which either $q^- \in \mathcal{R}(q^+)$ or $q^+ \in \mathcal{R}(q^-)$. In light of the foregoing discussion, we have the following result.

Proposition 1. *For each $q^+, q^- \in \mathcal{Q}$ there exists a parametric* VHC *$q = \sigma(\theta)$ connecting q^+ and q^- (i.e., for some $\theta_a, \theta_b \in \mathbb{R}$, $\sigma(\theta_a) = q^+$ and $\sigma(\theta_b) = q^-$) if, and only if, q^+ and q^- do not belong to a common orbit of g_{acr}, i.e., $q^- \notin \mathcal{O}^{g_{acr}}(q^+)$.*

Proposition 1 gives a conclusive answer to whether MP is solvable for the acrobot, and it furnishes a practical test: for a leg aperture β, determine q^+ and q^- from (3). Plot the orbit of g_{acr} through q^+. If, and only if, q^- does not lie on this orbit, then a parametric VHC exists that connects q^+ and q^-. Note, however, that we also require the VHC curve to be entirely contained in the safe set $\mathcal{W}$. We do not investigate this requirement theoretically in this paper (although we take full account of it when investigating hybrid invariance in the next section). Instead, we will pose it as a constraint in the optimal control formulation of Section VIII.

VII. Hybrid Invariance

In the previous section we have determined when there exists a parametric VHC connecting two points $q^+, q^- \in \mathcal{Q}$. We now assume that for a given leg aperture β, the vectors q^+ and q^- given in (3) satisfy the conditions of Proposition 1, and we investigate the hybrid invariance specification G.B of the gait generation problem. Recall that we also need to avoid Zeno solutions of the hybrid constrained dynamics by ensuring that $\delta > 0$. We assume f_{acr} has been chosen so that $q^- \in \mathcal{R}(q^+)$ (if not, we reverse the sign of f_{acr}).

Much work on bipedal locomotion uses VHCs described by Bézier polynomials, in which case it is shown in [12] that hybrid invariance can be enforced by means of certain constraints on the coefficients of the polynomials. These constraints amount to imposing requirements on the slopes of the VHC curve at its endpoints. In this section we explore this idea further for generic parametric VHCs, and we show that hybrid invariance can be enforced by fixing the initial and final values of the virtual control signal in the VCG.

We start from the hybrid invariance condition C1 which requires that when $(q^-, \dot{q}^-) \in \Gamma$, we must have $\Delta(q^-, \dot{q}^-) \in \Gamma$, or

$$\begin{aligned} q^+ &= R(q^-) \\ \dot{q}^+ &= -\Omega(q^-)\dot{q}^-. \end{aligned}$$

The first condition is met by construction: we have built it into our problem statement (specification G.A), and we have given necessary and sufficient conditions for its feasibility in Proposition 1. As for the second identity, using the fact that $\Sigma : (\theta, \dot{\theta}) \mapsto (\sigma(\theta), \sigma'(\theta)\dot{\theta})$ is a diffeomorphism $\mathbb{R} \times \mathbb{R} \to \Gamma$, we rewrite the identity as

$$\sigma'(\theta_a)\dot{\theta}_a = -\Omega(q^-)\sigma'(\theta_b)\dot{\theta}_b. \tag{21}$$

The matrix $-\Omega(q^-)$ is fixed by the choice of β, and the unknowns are the tangent vectors to the VHC curve at its endpoints, $\sigma'(\theta_a)$ and $\sigma'(\theta_b)$. Once these are determined, the ratio $\dot{\theta}_a/\dot{\theta}_b$ is the nonzero constant δ defined in (17).

Let $t(\theta)$ denote the unit tangent vector to the curve $q = \sigma(\theta)$, i.e., $t(\theta) := \sigma'(\theta)/\|\sigma'(\theta)\|$. From (21) we deduce that $t(\theta_a) = -\lambda\Omega(q^-)t(\theta_b)/\|\Omega(q^-)t(\theta_b)\|$, where $\lambda \in \{+1, -1\}$ is the sign of the ratio $\delta = \dot{\theta}_a/\dot{\theta}_b$. Specification G.B requires $\delta > 0$, so we impose $\lambda = 1$, which gives

$$t(\theta_a) = \Theta(t(\theta_b)) := -\frac{\Omega(q^-)t(\theta_b)}{\|\Omega(q^-)t(\theta_b)\|}. \tag{22}$$

We have found $t(\theta_a)$ in terms of $t(\theta_b)$. Next, we need to determine $t(\theta_b)$. There are two restrictions on this quantity.

First, both tangent vectors $t(\theta_b)$ and $t(\theta_a) = \Theta(t(\theta_b))$ must satisfy the transversality requirement (13) of a regular VHC, i.e., be transversal to the subspace $\text{Im}(D^{-1}B)$. Further, since $\sigma(\theta)$ is a solution of the VCG, the tangent vectors to this curve must point to the same side of the line $\text{Im}(D^{-1}B)$ as f_{acr} does. In other words, letting[5] $\mu := \text{sign}\left(\det\begin{bmatrix} f_{\text{acr}} & g_{\text{acr}}\end{bmatrix}\right)$, we require the vectors $t(\theta_b)$ and $t(\theta_a) = \Theta(t(\theta_b))$ to satisfy

$$\mu \det\begin{bmatrix} t(\theta_b) & D^{-1}(q^-)B\end{bmatrix} > 0 \tag{23a}$$

$$\mu \det\begin{bmatrix} \Theta(t(\theta_b)) & D^{-1}(q^+)B\end{bmatrix} > 0. \tag{23b}$$

Second, the curve $q = \sigma(\theta)$ must be **compatible with the safe set $\mathcal{W}$ at its endpoints**. By this we mean, referring to Figure 3, that the tangent vector $t(\theta_b)$ should point to the exterior of the safe set $\mathcal{W}$, and the vector $t(\theta_a)$ should point to the interior of $\mathcal{W}$. Letting $n = -\begin{bmatrix}2 & 1\end{bmatrix}^\top$ be the normal vector to the boundary lines $q_2 = -2q_1$ and $q_2 = -2q_1 + 2\pi$, the compatibility requirement translates to the conditions

$$\langle t(\theta_b), n\rangle \geq 0, \ \langle \Theta(t(\theta_b)), n\rangle \geq 0. \tag{24}$$

Now we bring in the VCG (20), and characterize specification G.B in terms of the virtual control values $u_a = u(\theta_a)$, $u_b = u(\theta_b)$ at the beginning and end of the step. Imposing that $\sigma(\theta)$ be a solution of (20), we have

$$\sigma'(\theta_b) = f_{\text{acr}} + g_{\text{acr}}(q^-)u_b = \begin{bmatrix} f_{\text{acr}} & g_{\text{acr}}(q^-)\end{bmatrix}\begin{bmatrix}1 \\ u_b\end{bmatrix}. \tag{25}$$

[5]The function μ is constant on $\mathcal{Q}$ because $f_{\text{acr}}, g_{\text{acr}}$ are everywhere transversal.

The matrix in (25) is invertible. Expressing the left-hand side of the above identity as $\sigma'(\theta_b) = \|\sigma'(\theta_b)\| t(\theta_b)$, we solve equation (25) as follows:

$$\frac{1}{\|\sigma'(\theta_b)\|}\begin{bmatrix}1\\ u_b\end{bmatrix} = \begin{bmatrix} f_{\text{acr}} & g_{\text{acr}}(q^-)\end{bmatrix}^{-1} t(\theta_b). \tag{26}$$

This identity gives $\|\sigma'(\theta_b)\|$ and u_b in terms of $t(\theta_b)$. Using (22) and repeating the foregoing considerations for the vector $\sigma'(\theta_a)$, we get $\|\sigma'(\theta_a)\|$ and u_a:

$$\frac{1}{\|\sigma'(\theta_a)\|}\begin{bmatrix}1\\ u_a\end{bmatrix} = \begin{bmatrix} f_{\text{acr}} & g_{\text{acr}}(q^+)\end{bmatrix}^{-1} \Theta(t(\theta_b)). \tag{27}$$

We summarize the development so far. Given a leg aperture β, we compute q^+, q^- using (3). We select $t(\theta_b) \in \mathbb{S}^1$ such that conditions (23) and (24) hold. This choice in particular implies that the constant $\delta = \dot\theta_a/\dot\theta_b$ is positive, avoiding Zeno solutions. If there is no choice of $t(\theta_b) \in \mathbb{S}^1$ satisfying (23) and (24), then the gait generation problem is unsolvable for the given leg aperture β, and we must select a different β. If instead there is a choice of $t(\theta_b) \in \mathbb{S}^1$ satisfying (23)-(24), then we compute $t(\theta_a)$ from (22), and u_a, and u_b from (26) and (27). Any solution $q = \sigma(\theta)$ of the VCG connecting q^+ and q^- will give rise to a parametric VHC satisfying the hybrid invariance conditions provided that the initial and final values of the virtual control signal are u_a and u_b, respectively. These considerations are summarized in the next result.

Proposition 2. *Let $q^+, q^- \in \mathcal{Q}$ satisfy the hypothesis of Proposition 1 and suppose that $q^- \in \mathcal{R}(q^+)$. Then there exists a parametric* VHC *$q = \sigma(\theta)$ that connects q^+ and q^-, satisfies the hybrid invariance specification* G.B*, and is compatible at its endpoints with the safe set $\mathcal{W}$ if, and only if, there exists $t(\theta_b) \in \mathbb{S}^1$ satisfying conditions* (23) *and* (24)*. Moreover, this* VHC *can be generated as a solution of the* VCG (20) *provided the initial and final values of the virtual control input signal are the ones given in* (26) *and* (27)*.*

Although Proposition 2 concerns the acrobot, the result can be generalized to planar walking robots with degree of underactuation one and its essence would remain unchanged. Namely, imposing hybrid invariance for a VHC is mathematically equivalent to imposing conditions on the initial and final values of the virtual control signal of the VCG generating the VHC in question.

VIII. Optimal control formulation

Having given theoretical characterizations of the feasibility of specifications G.A and G.B in the gait generation problem (with the exception of the safety requirement in G.A), we are ready to synthesize walking gaits.

Recall that the set of embedded curves that are solutions of the VCG (20) coincides with the set of all parametric VHCs modulo reparametrization so designing a walking gait amounts to designing a controller for the VCG. In this section we formulate an optimal control problem for the VCG with an objective functional of the form $J(\theta_b, \sigma, u)$, where $\theta_b > \theta_a$ is the variable time horizon of the problem (we pick $\theta_a = 0$ for simplicity), and $\sigma(\cdot)$ is a solution of the VCG (20) with control input signal $u(\cdot) \in \mathcal{U}$, the set of twice differentiable control signals $[\theta_a, \theta_b] \to \mathbb{R}$. The optimal control signal $u(\cdot)$ is subject to these constraints:

(a) For some[6] $\theta_b > 0$, $\sigma(\theta_b) = q^-$.
(b) The VHC curve $q = \sigma(\theta)$ is contained in the region $\mathcal{W}$ as defined in G.A for $\theta \in (\theta_a, \theta_b)$.
(c) The virtual mass and potential induced by the VHC satisfy the existence and stability conditions (19b):

$$0 < \frac{\delta^2}{M(\theta_b)} < 1, \quad \frac{V(\theta_b)\delta^2}{M(\theta_b) - \delta^2} + V_{\max} < 0.$$

While requirements (a) and (b) can be readily formulated as constraints in an optimal control problem for the VCG, requirement (c) and possibly the objective functional are not ready for the formulation because they have not yet been connected to the VCG. More precisely, we need to express $M(\theta_b)$, $V(\theta_b)$, and $V_{\max}$ in terms of the VCG state and virtual control input. To this end, we note that the virtual mass and potential induced by a parametric VHC $q = \sigma(\theta)$ depend on the functions Ψ_1, Ψ_2 in (15), which in turn depend on σ, σ', and σ''. Since $\sigma(\theta)$ is a solution of (20), we have, omitting the argument θ,

$$\begin{aligned}\sigma' &= f_{\text{acr}} + g_{\text{acr}}(\sigma)u\\ \sigma'' &= (dg_{\text{acr}})_\sigma\, \sigma' u + g_{\text{acr}}(\sigma)u'.\end{aligned}$$

Substituting the expression of σ' from the first identity into the second identity we get

$$\sigma'' = (dg_{\text{acr}})_\sigma \big(f_{\text{acr}} + g_{\text{acr}}(\sigma)u\big)u + g_{\text{acr}}(\sigma)u'.$$

We see that the derivatives σ' and σ'' can be expressed in terms of σ, u, and u', and that u' appears in σ'' only. Moreover, σ'' affects the function Ψ_2 in (15b) via the term $B^\perp D\sigma''$, and since $g_{\text{acr}} = D^{-1}B$, $B^\perp D\sigma''$ is independent of u'. Similarly, the terms $B^\perp D\sigma'$ in Ψ_1 and Ψ_2 are independent of u.

In conclusion, substituting the expressions for σ' and σ'' above in the definitions of Ψ_1, Ψ_2 in (15), we obtain a function Ψ_1 parametrized by σ, and a function Ψ_2 parametrized by σ and u. We will denote these functions by $\Psi_1^\sigma(\theta)$ and $\Psi_2^{\sigma,u}(\theta)$, respectively. Using Ψ_1^σ and $\Psi_2^{\sigma,u}$ in (16), we obtain expressions for the virtual mass and potential parametrized by σ and u, and denoted $M^{\sigma,u}(\theta)$, $V^{\sigma,u}(\theta)$, respectively. We may now express the constraint (19) for existence and stability of a hybrid limit cycle in terms of the VCG solution $\sigma(\theta)$ and input signal $u(\theta)$. Similarly, in the objective functional J we may use terms dependent on the virtual mass and potential M and V because these can be expressed in terms of $\sigma(\theta)$ and $u(\theta)$.

We now formally pose the finite horizon optimal control problem with variable terminal time θ_b (and $\theta_a = 0$). We select a leg aperture β so that the assumptions of Propositions 1 and 2 hold. We compute q^+ and q^- from (3), and u_b, u_a from (26)-(27) after having chosen $t(\theta_b)$ satisfying conditions (23) and (24). Using (26)-(27) and (22), we also get the vectors $\sigma'(\theta_a)$ (where $\theta_a = 0$) and $\sigma'(\theta_b)$. Finally, from (17) we get δ. We express the safe set $\mathcal{W}$ in (4) as $\mathcal{W} = \{q \in \mathcal{Q} : I_j(q) \le 0,\ j = 1, \dots, 4\}$, with

$$\begin{aligned} I_1(q) &= q_2 + 2q_1 - 2\pi, & I_2(q) &= -2q_1 - q_2\\ I_3(q) &= -q_1, & I_4(q) &= q_1 - \pi.\end{aligned}$$

[6]By our choice of f_{acr}, q^- is contained in the set of points reachable from q^+ in positive time and so $\theta_b > 0$.

OPTIMAL CONTROL PROBLEM.

$$\underset{(\theta_b,u)\in(\theta_a,\infty)\times\mathcal{U}}{\text{minimize}} \; J(\theta_b, u) \tag{28}$$

$$\text{subject to } \frac{d\sigma}{d\theta} = f_{\text{acr}}(\sigma(\theta)) + g_{\text{acr}}(\sigma(\theta))u(\theta) \tag{29}$$

$$\sigma(\theta_a) = q^+ \tag{30}$$

$$\sigma(\theta_b) = q^- \tag{31}$$

$$u(\theta_a) = u_a \tag{32}$$

$$u(\theta_b) = u_b \tag{33}$$

$$\delta^2 V^{\sigma,u}(\theta_b)/\big(M^{\sigma,u}(\theta_b) - \delta^2\big) + \max_{\theta\in[0,\theta_b]} V^{\sigma} < -\varepsilon \tag{34}$$

$$\varepsilon_1 < \delta^2/M^{\sigma,u}(\theta_b) < 1 - \varepsilon_2 \tag{35}$$

$$I_j(\sigma(\theta)) \le 0, \;\; \theta \in (0, \theta_b), \;\; j = 1, \ldots, 4, \tag{36}$$

where $\varepsilon, \varepsilon_1, \varepsilon_2 > 0$ are small design parameters and $\theta_a = 0$. This problem seeks a solution of the VCG minimizing the objective functional under a number of constraints. Identity (30) is the initial state of the VCG, while (31) is the target state. Identities (32) and (33) impose initial and final values for the virtual control guaranteeing hybrid invariance. Inequalities (34)-(35) ensure the existence and stability of a hybrid limit cycle, while the inequalities (36) ensure that the solution remains in the safe set $\mathcal{W}$.

The well-posedness of this optimal control problem has been partially addressed in Propositions 1 and 2. The parts we have not characterized theoretically are the existence of a solution meeting (34) and (36). In the next section, we solve the optimal control problem numerically using the direct collocation method of [39].

We emphasize that the leg aperture β and the endpoint tangent vector $t(\theta_b)$ could be included in the set of optimization parameters, as opposed to being fixed a priori.

IX. SIMULATION RESULTS

In this section we provide a high-level description of the numerical procedure stemming out of the optimal control formulation of Section VIII, and present the resulting walkover gait. Throughout this section, we assume that there is a holonomic constraint keeping the stance foot pinned during the swing phase, such as the mechanism discussed at the beginning of Section II.

NUMERICAL GAIT SYNTHESIS PROCEDURE

1. Select a leg aperture $\beta \in (0, \pi)$ and compute q^+, q^- according to (3).

2. Using Proposition 1, verify that there exists a VHC curve connecting q^+ and q^-. This amounts to verifying that q^+ and q^- are not on a common orbit of g_{acr}. If the verification gives a negative result, **stop**. The gait generation problem is unsolvable for the given β.

3. Compute[7] the time it takes for the solution of f_{acr} through q^+ to reach the orbit of g_{acr} through q^-. The result of this computation is an initialization for the variable θ_b. If $\theta_b < 0$, replace f_{acr} by $-f_{\text{acr}}$, replace θ_b by its absolute value, and continue.

4. Select a unit vector $t(\theta_b)$ satisfying (23) and (24). If no such quantity exists, **stop**. The gait generation problem is unsolvable for the given β.

5. Using (22), compute $t(\theta_a)$, and using (26) and (27), compute $\|\sigma'(\theta_b)\|$, $\|\sigma'(\theta_a)\|$, u_a, u_b. Set $\sigma'(\theta_b) = \|\sigma'(\theta_b)\| t(\theta_b)$ and $\sigma'(\theta_a) = \|\sigma'(\theta_a)\| t(\theta_a)$, then compute δ using (17).

6. Set up the optimal control problem of Section VIII using direct collocation. Initialize it with θ_b from step 3 and a constant control signal $\bar{u} \in \mathcal{U}$ found by performing a 1-dimensional search over constant controls for a solution of the VCG connecting q^+ to q^-. (This search is guaranteed to terminate successfully [37], and the constant control is unique).

7. The output of the direct collocation algorithm is a piecewise constant control signal $u(\theta)$. Find the resulting solution[8], $\sigma(\theta)$, of the VCG. The curve $q = \sigma(\theta)$ is a parametric VHC for the acrobot inducing a stable hybrid limit cycle that corresponds to a stable walkover gait.

TABLE I: Acrobot parameters

Parameter	
m	0.3 kg
l_c	0.5 m
l	1 m
I_z	0.025 kg·m^2

In our simulations, we explored a variety of objective functionals $J(\theta_b, \sigma, u)$. We present results for two functionals of the form $J(\theta_b, \sigma, u) = J_i(\theta_b, \sigma, u) + \gamma\, J_{\text{reg}}(u)$, where

$$J_1(\theta_b, \sigma, u) = \int_{\theta_a}^{\theta_b} \|\sigma'(\theta)\| d\theta$$

$$J_2(\theta_b, \sigma, u) = 1/M^{\sigma,u}(\theta_b)$$

$$J_{\text{reg}}(u) = \left(\int_{\theta_a}^{\theta_b} \|u''(\theta)\|^2 d\theta \right)^{1/2},$$

and $\gamma > 0$ is a design parameter.

The functional J_1 represents the length of the VHC curve. Minimizing it gives VHC curves that are not too far from the straight line segment connecting q^+ and q^-. This has the effect of avoiding kicking behaviours in the gait. The functional J_2 is proportional[9] to the absolute value of the eigenvalue of the linearized Poincaré map of the hybrid constrained dynamics, $\big|\delta^2/M(\theta_b)\big|$. Minimizing it gives VHC curves that induce faster convergence to the hybrid limit cycle. The functional $J_{\text{reg}}(u)$ in both costs is a regularizing term that smooths out the control

[7] One can check that $[f_{\text{acr}}, g_{\text{acr}}] = 0$, and by Theorem 1 in Appendix B, this implies that the time it takes for solutions of the VCG to transition between any two orbits of g_{acr} is independent of the choice of virtual control u. To compute θ_b, set $u(\theta) \equiv 0$ and find the time $\bar{\theta}$ it takes for the solution of the VCG (i.e., the integral curve of f_{acr}) initialized at $q(0) = q^+$ to reach the orbit of g_{acr} through q^-, $\mathcal{O}^{g_{\text{acr}}}(q^-)$; then set $\theta_b = \bar{\theta}$.

[8] More precisely, the function σ is found through spline interpolation of the samples of the numerical solution of the VCG with initial condition $\sigma(0) = q^+$ and piecewise continuous control signal $u(\theta)$. Some care must be taken with the spline interpolation to ensure that the resulting σ respects hybrid invariance. In MATLAB this can be done by providing the initial and final slopes found in step 5, $\sigma'(\theta_a)$ and $\sigma'(\theta_b)$, to the `spline()` command.

[9] We recall that the function $M^{\sigma,u}$ in the definition of J_2 is the virtual mass expressed in terms of the VCG state and control input, presented in Section VIII.

signal by weighing the L_2 norm of the second derivative of u.

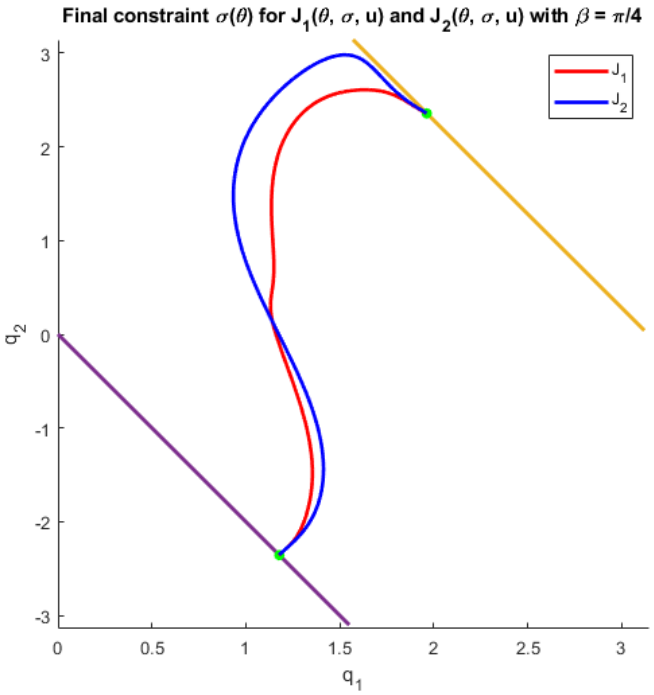

Fig. 6: VHC curves resulting from optimization of the objective functionals $J_1 + J_{\text{reg}}$ (path length, shown in red) and $J_2 + J_{\text{reg}}$ (eigenvalue of the linearized Poincaré map, shown in blue) with leg aperture $\beta = \pi/4$. A video of the dynamic simulation of the gait corresponding to J_1 is available at https://play.library.utoronto.ca/watch/fb4086187d812b92edac9b39c98761bb

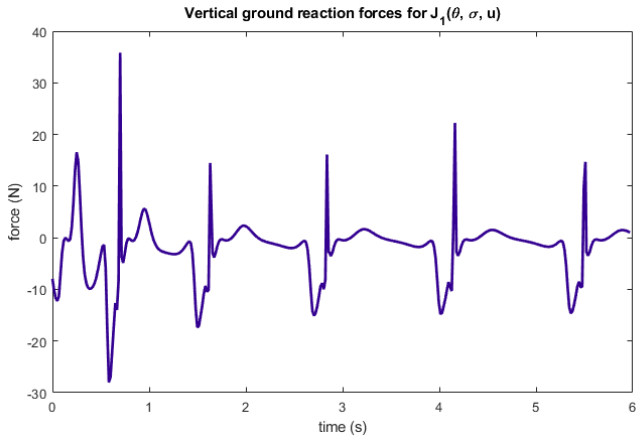

Fig. 7: Vertical ground reaction forces for the gait corresponding to the red constraint in Figure 6. The system is initialized off the constraint and converges to the stable hybrid limit cycle. A negative ground reaction force indicates that the stance foot would lift from the ground, causing the acrobot to jump.

Using the model parameters summarized in Table I (close to those used in [13]), we find that a leg aperture $\beta = \pi/4$ is feasible. Following the procedure above for the two objective functions J_1 and J_2, we get the constraint curves depicted in Figure 6. These constraints meet all specifications of the gait generation problem and produce stable hybrid limit cycles for the walkover gait.

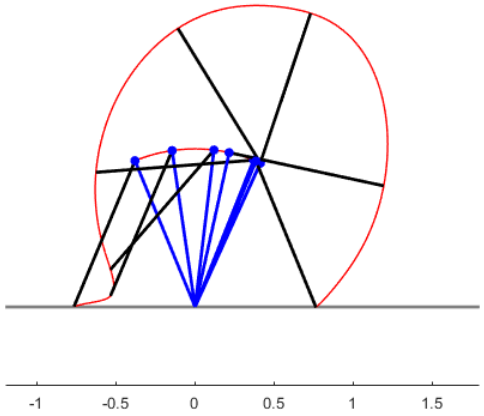

Fig. 8: Acrobot configurations along the VHC of Figure 6 corresponding to the objective functional $J_1 + J_{\text{reg}}$ (path length) for $\beta = \pi/4$. The blue line represents the stance leg, while the black line represents the swing leg. The red lines show the path of the hip and swing foot over the step.

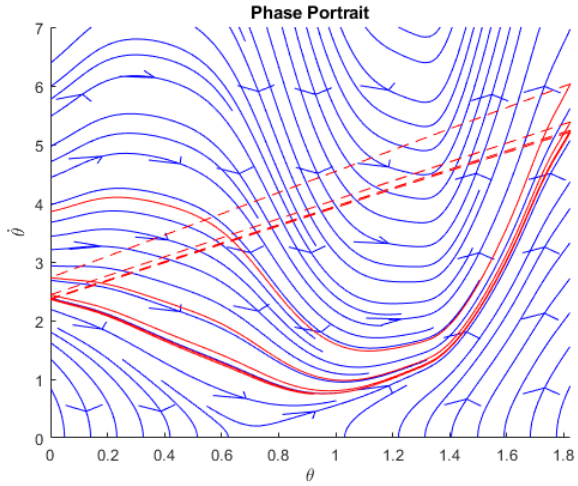

Fig. 9: Phase portrait of the reduced walkover dynamics induced by the red constraint in Figure 6. The portrait shows convergence to the stable hybrid limit cycle. The dashed lines indicate state jumps due to ground impacts.

The configurations of the acrobot on the constraint set for the objective function J_1 are displayed in Figure 8. Near the beginning of the step, the VCG inputs for hybrid invariance keep the swing foot motion relatively close to the floor. During the middle portion of the step, the swing leg swings up and over the stance leg. Partway through this swingover motion, the hip flicks backwards to bring the swing foot down. The motion on the constraint manifold Γ for the constraint associated with the objective function J_1 is shown in Figure 9,

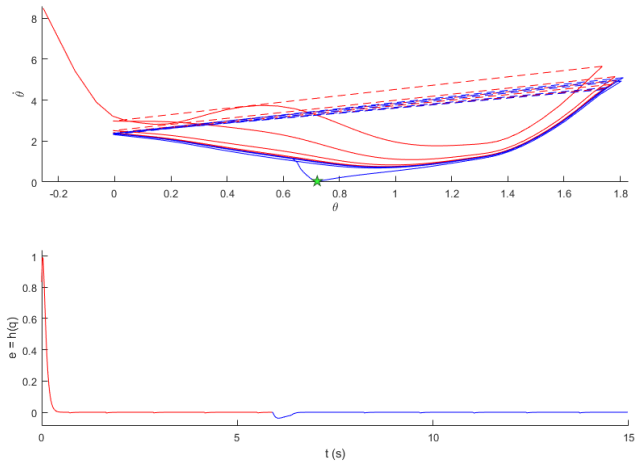

Fig. 10: Effects of a sudden disturbance applied from $t = 5.9\,\text{s}$ to $t = 6.35\,\text{s}$ during step 6, using the VHC associated with J_1 in Figure 6. The first subplot shows the projection of the state trajectory on the constraint manifold, while the second subplot shows the VHC error signal $e(t) = h(q(t))$. In both subplots, red lines correspond to the solution before the disturbance is applied ($t < 5.9\,\text{s}$), while blue lines correspond to times after the disturbance has appeared ($t \geq 6.35\,\text{s}$). Following the disturbance, during step 7 the signal $\dot{\theta}(t)$ gets close to zero (see point $\star$ in the figure) meaning that the robot comes temporarily to a halt. The robot then recovers and quickly converges to the stable hybrid limit cycle. The video of this simulation is available at https://play.library.utoronto.ca/watch/2ff9e40ae60ba9c2318b2d846338b219.

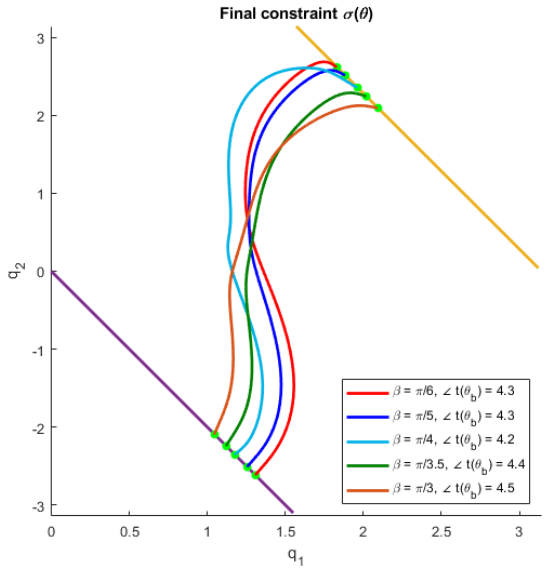

Fig. 11: VHC curves resulting from the optimization of the objective functional $J_1 + J_{\text{reg}}$ for different values of the leg aperture β.

along with a sample solution showing convergence to the hybrid limit cycle over multiple steps. Results for the cost J_2 are similar. Note that smoothing the final constraint, as in Figure 6, may result in slight variations in $M^{\sigma,u}(\theta_b)$, $V^{\sigma,u}(\theta_b)$, and $V_{\max}$. It is therefore necessary to check that the existence and stability conditions continue to be satisfied for the smoothed constraint.

It should be noted that the optimal control formulation used in our simulations does not impose any requirements on the ground reaction forces at the stance foot. As such, gaits produced with the current formulation are not guaranteed to keep the stance foot pinned to the ground. The constraints in Figure 6 and Figure 11 all induce gaits for which the ground reaction forces point downwards at some point during the step. In other words, without a mechanism in place to keep the stance foot pinned, the stance foot would lift from the ground. In fact, for the orange constraint in Figure 11 corresponding to $\beta = \pi/3$, it is possible for the method above to produce a constraint such that the ground reaction forces point downwards for the entire duration of the step. Such a constraint is therefore not feasible without a method of pinning the stance foot to the ground. In Section X, we discuss a method of augmenting the current formulation to enforce ground reaction forces, which will be the subject of future work.

Figure 10 shows how the acrobot recovers from the effects of a sudden disturbance of finite duration acting during step 6 between $t = 5.9\,\text{s}$ and $t = 6.35\,\text{s}$, and bringing the robot almost to a halt during step 7. The VHC used in this simulation is the one depicted in Figure 6 associated with the objective functional J_1. The disturbance causes the robot's state to leave the constraint manifold, but the robot quickly recovers and converges again to the hybrid limit cycle. This simulation is in line with observations conducted by other researchers using VHCs to control biped robots, e.g., the robot Atrias in [22].

Figure 11 depicts constraints obtained with the objective function J_1 for different values of β. All these constraints induce stable walkover gaits, but not all of them produce ground reaction forces keeping the stance foot pinned to the ground.

Finally, the method developed in this paper produces stable walking gaits for *uphill* walking, a particularly challenging problem in the literature, especially for a robot with just two DOFs. Figure 12 presents a VHC obtained when the ground has an uphill slope of 2 degrees. The objective function is J_1 and the leg aperture is $\pi/4$.

In our simulations we noticed some sensitivity to the choice of $t(\theta_b)$: for the same set of acrobot parameters and choice of β, some choices for $t(\theta_b)$ produced stable gaits while others produced infeasible constraint curves. This may also be a consequence of using direct collocation to perform the optimization.[10]

[10]The constraints in Figure 11 took between 36 and 120 seconds to generate on a computer with a 3.4 GHz Intel i7 CPU. Note that the code used to generate these constraints is not optimized, and utilizes our own implementation of direct collocation using the MATLAB function `fmincon()`. Note also the time needed to generate a constraint varies with the acrobot and gait parameters, the guess used to initialize `fmincon()`, and the choice of `fmincon()` algorithm.

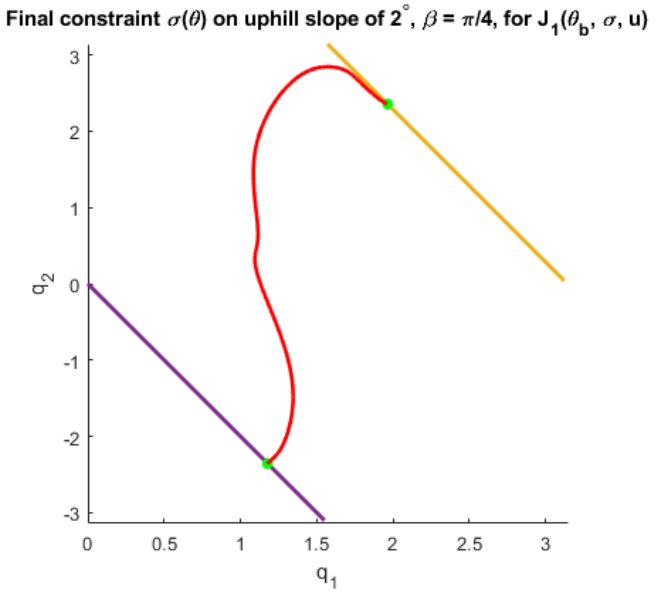

Fig. 12: VHC curve resulting from the optimization of the objective functional $J_1 + J_{\text{reg}}$ and $\beta = \pi/4$ when the ground has an uphill slope of 2 degrees. The video of this simulation is available at https://play.library.utoronto.ca/watch/eac6339518d0ea2a8847bd5dc96b5e14

X. Practical considerations

In this section we discuss practical details related to the numerical implementation of the VCG-based gait design algorithm presented in Sections VIII and IX.

Numerical integration. The optimal control problem posed in Section VIII requires the numerical integration of the VCG. For the evaluation of the virtual mass and potential functions, $M^{\sigma,u}$ and V^{σ}, used in the optimization constraints (34) and (35) and in the cost functional J_2, one can augment the state of the VCG with two states, M and V, obtaining the augmented VCG dynamics

$$\begin{aligned} \frac{d\sigma}{d\theta} &= f_{\text{acr}}(\sigma(\theta)) + g_{\text{acr}}(\sigma(\theta))u(\theta) \\ \frac{dM}{d\theta} &= -2\Psi_2^{\sigma,u}(\theta)M(\theta) \\ \frac{dV}{d\theta} &= -\Psi_1^{\sigma}(\theta)M(\theta), \end{aligned} \tag{37}$$

where Ψ_1^{σ} and $\Psi_2^{\sigma,u}$ are the functions presented in Section VIII. System (37) has $n+2$ states, where n is the number of DOFs of the robot ($n = 2$ for the acrobot). The direct collocation method discretizes the dynamics in (37) and the control input u, giving optimization parameters $(\sigma(\theta_i), M(\theta_i), V(\theta_i), u(\theta_i))_{i=1,\dots,N} \in \mathbb{R}^{N(n+3)}$ (where N is the number of collocation points), subject to constraints arising from the discretization of the optimization constraints in (29).

Taking into account ground reaction forces. There are two types of ground reaction forces: the one acting on the stance foot during the swing phase and the impulsive reaction force at the swing foot during the impact phase. From a practical perspective, there are requirements on these forces. The reaction force at the stance foot must not make the foot lift off the ground or slip, while the impulsive reaction force at the swing foot must satisfy the no slip and no rebound assumption used in the modelling. As explained in the book [12], these two requirements can be expressed in terms of inequality constraints involving the signals $(q(t), \dot{q}(t), \ddot{q}(t))$ when the robot state is on the hybrid limit cycle. These signals are available in our optimal control formulation provided the VCG is dynamically extended with $n-1$ parallel integrators at the input side:

$$\begin{aligned} \frac{d\sigma}{d\theta} &= f_{\text{acr}}(\sigma(\theta)) + g_{\text{acr}}(\sigma(\theta))\xi(\theta) \\ \frac{d\xi}{d\theta} &= v(\theta), \end{aligned} \tag{38}$$

where $v \in \mathbb{R}^{n-1}$ is the new control input.

More in detail, we return to the reasoning of Section VIII. If $(q(t), \dot{q}(t)) \in \Gamma$ for all $t \geq 0$, then $q(t) = \sigma(\theta(t))$. Using the fact that $\sigma(\theta)$ is a solution of the VCG (20), we showed in Section VIII that $(q(t), \dot{q}(t), \ddot{q}(t))$ can be expressed in terms of $(\sigma(\theta), u(\theta), u'(\theta))$. In terms of the extended VCG (38), we have $(\sigma(\theta), u(\theta), u'(\theta)) = ((\sigma(\theta), \xi(\theta), v(\theta)))$. By using system (38) in place of the VCG in the optimal control formulation (29), one can include optimization constraints imposing requirements on the ground reaction forces.

Constraint implicitization. Our VCG-based gait design produces parametric VHCs $q = \sigma(\theta)$ resulting from a search in the space of all regular VHCs. This is a feature that distinguishes it from other approaches in the literature, and we will return to it in Section XI. To implement the controller $\tau^\star$ in Section IV-A, one needs to express the VHC $q = \sigma(\theta)$ in implicit form as $h(q) = 0$. There are two ways to do this. The simplest way is to attempt to express the curve $q = \sigma(\theta)$ as the graph of a function in $\mathcal{Q}$ after an appropriate coordinate transformation. This is what we do in all our simulations. If this approach is not viable, then one can use polynomial approximations of the function σ and the implicitization algorithm presented in [40, Ch.4].

Implementation using servomotors. Many small robots are actuated via servomotors, in which case neither the motor terminal voltages nor the armature currents are available as control inputs because the motors have PID control loops within. The control inputs in this case are the reference signals for the joint variables. The simplest approach to enforce the VHC $h(q) = 0$ is to express it as the graph of a function $(q_2, \dots, q_n) = \phi(q_1)$, after a suitable relabelling of the configuration variables. If joints $2, \dots, n$ are actuated, then the input sent to the servomotors is simply $\phi(q_1)$. This is the approach used, e.g., in [41]. For the acrobot, this amounts to expressing the VHC as $q_2 = \phi(q_1)$ and letting this expression be the control input sent to the servomotor. Some of the constraints presented in Section IX cannot be expressed as graphs of functions $q_2 = \phi(q_1)$, but the configuration plane $\mathcal{Q}$ can be partitioned into two or three regions $\mathcal{Q}_i \subset \mathcal{Q}$ over which one has a relationship $q_2 = \phi^i(q_1)$. The controller gets (q_1, q_2) from the sensors, determines the region $\mathcal{Q}_i$ that q is in, and commands the servomotor to the setpoint $q_2 = \phi^i(q_1)$.

Generality of the proposed approach. The optimal control formulation in Section VIII was developed for the acrobot

example, but is in fact generalizable to planar bipedal robots with point feet and degree of underactuation one. In this more general setting, the VCG is a control system on $\mathcal{Q}$, an n-dimensional configuration manifold, with $n-1$ control inputs. Hybrid invariance still amounts to imposing restrictions on the initial and final values of the virtual control input signal, $u(\theta_a)$ and $u(\theta_b)$. The optimal control formulation in (29) remains substantially unchanged. The idea presented in the earlier paragraph of extending the VCG so as to impose requirements on ground reaction forces is generally applicable and not restricted to the acrobot.

From a theoretical perspective, the generalization of Propositions 1 and 2 requires significant research, but the line of attack of dividing the gait generation problem into the subproblems G.A, G.B, and G.C would remain unchanged.

XI. Comparison to State-of-the-Art

In this section we compare our gait design philosophy (henceforth referred to as the **VCG approach**) with the approach presented in the book [12] (henceforth referred to as the **WesGri approach** after the last names of the first two authors) as well as the more recent approach of the FROST toolbox developed by Hereid and Ames [42]. We will refer to this latter as the **FROST approach**.

Both WesGri and FROST consider a specific class of parametric VHCs expressed by the relation

$$h(q) := h_0(q) - h^d(\tau(q), \alpha) = 0. \tag{39}$$

In the above, $h_0(q)$ is an output function, and h^d is a polynomial (typically a Bézier polynomial)[11] with parameter vector α. The function $\tau(q)$ is what in this paper we call the phase variable θ, and it represents a configuration-dependent timing variable that is desired to be monotonic along steady-state solutions. The problem of enforcing the VHC (39) can be interpreted as that of making the output $h_0(q)$ asymptotically track the reference "signal" h^d. In WesGri and FROST, designing a VHC amounts to finding the parameter vector α.

In WesGri, one poses a constrained optimization problem with an objective function $J(\alpha)$ subject to a variety of constraints the most important of which are:

(i) The VHC (39) must satisfy the regularity condition (12), i.e, the output $h(q)$ must yield relative vector degree $\{2, \cdots, 2\}$ on $h^{-1}(0)$.
(ii) The constraint must induce virtual mass and potentials meeting the conditions in (34), (35) for the existence of stable hybrid limit cycles.
(iii) Along the hybrid limit cycle, the ground reaction forces at impact must be consistent with the hypothesis of impact with no slip and no rebound.
(iv) Along the hybrid limit cycle, the ground reaction forces must be such that the stance leg remains pinned to the ground.

To evaluate the constraints, the nonlinear optimizer must compute for each α the virtual mass and virtual potential functions, the parameter δ of the reduced impact map, an initial condition on the hybrid limit cycle, and the feedback $\tau(q, \dot{q})$ enforcing the VHC. Then, the optimizer must simulate the $2n$ dimensional model of the pinned robot (where n is the number of DOFs of the robot) to get the signals $(q(t), \dot{q}(t), \ddot{q}(t))$ needed to compute the ground reaction forces. All in all, WesGri involves the simulation of a $2n + 2$-dimensional dynamical system, the model of the pinned robot plus two differential equations for the computation of the virtual mass and potential.

The costs $J(\alpha)$ proposed in [12] rely on the computation of the control input when the robot is on the limit cycle. From a theoretical perspective, this means that the cost is undefined outside the constraint set, and in particular when the optimization constraint (ii) is violated. This could pose a problem numerically because typical nonlinear optimizers need to violate the constraint during the search.

In FROST, the constrained optimization problem is formulated for the model of the *unpinned* robot which has dimension $2n+2$ in the case of planar robots. FROST, however, deals with general 3D robots, and allows for much more general problem formulations then either the WesGri or VCG approaches. In contrast to WesGri and similarly to the VCG approach, FROST formulates an optimal control problem for the unpinned robot, using direct collocation for its numerical solution. Like WesGri, FROST includes the optimization constraints (i)-(iv) in its formulation. From a theoretical perspective, the objective function in FROST is well-defined even when the optimization constraint (ii) is violated, therefore obviating the aforementioned numerical issue present in WesGri.

Just like WesGri and FROST, the VCG approach allows one to take into account the optimization constraints (i)-(iv) above (see Section X), although in our simulations we do not impose constraints (iii)-(iv).

Now we come to the main differences between the VCG approach proposed in this paper and either WesGri or FROST. We emphasize that the VCG approach of this paper is in its infancy and is presently only applicable to robots with degree of underactuation one. It cannot handle the general classes of problems that FROST does. For instance, a robot with non-point feet has multi-foot contact behaviours that FROST can handle while the VCG approach cannot.

In the VCG approach, the constraints are solutions of an $n+2$ dimensional dynamical system, the VCG augmented with two differential equations for the computation of the virtual mass and potential. If ground reaction forces are to be taken into account in the optimization, then as discussed in Section X the dynamical system is $2n + 1$ dimensional.

In the VCG approach, the optimization is performed over the space $\mathcal{U}$ of twice differentiable virtual control signals (which is then discretized when setting up direct collocation). Searching the space $\mathcal{U}$ is equivalent to searching the space of *all* regular parametric VHCs for the given mechanical system. On the other hand, both WesGri and FROST perform the optimization over the set of parameters[12] of the polynomials h^d in (39). The regularity condition (12) is not built-in, and

[11] Note that FROST allows for several other classes of curves in addition to polynomials.

[12] FROST optimizes not just over the polynomial parameters, but many other parameters not directly related to the geometry of the VHC curve and arising from direct collocation.

it is imposed as an inequality constraint for the nonlinear program. More importantly, searching the parameter space of the polynomials in WESGRI and FROST does not correspond to searching the space of all possible regular VHCs. While WESGRI and FROST require the designer to choose an output function $h_0(q)$ and a timing variable $\tau(q)$, the VCG approach does not impose any such restriction, and the timing variable, θ in our framework, is found automatically by the algorithm as the parameter of the VHC curve. This feature could be useful when hunting for gaits for which not enough intuition is available to fix $h_0(q)$ and $\tau(q)$ a priori. The walkover gait is such an example.

To further elaborate on the point above, the VCG approach produces parametric constraints of the form $q = \sigma(\theta)$. There is no restriction on the structure of the function σ, other than the regularity requirement (12). On the other hand, WESGRI and FROST produce parametric constraints of the form (39) (FROST also considers relative degree one constraints used to impose speed specifications). It is clear that these constraints have a predetermined structure, and the phase variable $\theta = \tau(q)$ is chosen a priori.

Finally, in WESGRI and FROST hybrid invariance is enforced by imposing relationships between the coefficients of the Bézier polynomials parametrizing the constraint, whereas in this paper hybrid invariance is translated into a requirement for the initial and final values of the virtual control inputs.

XII. CONCLUSION

We have presented a procedure to generate virtual holonomic constraints inducing a stable walking gait for the acrobot corresponding to a walkover gait on flat ground and for shallow inclines. The ideas presented in this paper can be adapted to investigate other walking gaits for the acrobot, including but not limited to compass gaits. To illustrate, one could imagine gaits where the swing leg performs a fixed number of revolutions around the stance leg before impacting the ground. Future research will be devoted to generalizing the ideas of this paper to planar walking robots. It would also be desirable to compare from a computational viewpoint the gait generation method proposed in this paper to the other existing methods reviewed in Section XI.

APPENDIX A
IMPACT MAP QUANTITIES

Below are the matrices for the map Δ_1 in Section III.

$$D_e = \left[\begin{array}{cc|cc} \multicolumn{2}{c|}{\multirow{2}{*}{D}} & d_{13} & d_{14} \\ & & d_{23} & d_{24} \\ \hline d_{13} & d_{23} & \multicolumn{2}{c}{\multirow{2}{*}{$2mI_2$}} \\ d_{14} & d_{24} & & \end{array}\right]$$

$$d_{13} = (-lm - l_c m)s_{q_1} - l_c m s_{q_1+q_2}$$
$$d_{14} = (lm + l_c m)c_{q_1} + l_c m c_{q_1+q_2}$$
$$d_{23} = -l_c m s_{q_1+q_2}$$
$$d_{24} = l_c m c_{q_1+q_2}$$
$$E = \begin{bmatrix} -ls_{q_1+q_2} - ls_{q_1} & -ls_{q_1+q_2} & 1 & 0 \\ lc_{q_1+q_2} + lc_{q_1} & lc_{q_1+q_2} & 0 & 1 \end{bmatrix}.$$

APPENDIX B
A PROPERTY OF COMMUTING VECTOR FIELDS

Theorem 1. *Consider the planar single-input control system on the plane*

$$\dot{q} = f(q) + g(q)u(t), \tag{40}$$

where $f, g : \mathbb{R}^2 \to T\mathbb{R}^2$ are C^1 vector fields such that $[f, g] = 0$. Let $q^0 \in \mathbb{R}^2$ be arbitrary, and let $\Phi_t^{f+g\,u(t)}(q^0)$ denote the unique solution of (40) *with initial condition $q(0) = q^0$ and a piecewise continuous control signal $u : \mathbb{R} \to \mathbb{R}$. Assume that for each piecewise continuous $u : \mathbb{R} \to \mathbb{R}$, this solution is defined for all $t \geq 0$. Then for each $T \geq 0$ and any two piecewise continuous control signals $u^1(t)$ and $u^2(t)$, the points $\Phi_T^{f+g\,u^1(t)}(q^0)$ and $\Phi_T^{f+g\,u^2(t)}(q^0)$ belong to the same orbit of g, i.e.,*

$$(\forall T > 0)(\forall u^1, u^2 : \mathbb{R} \to \mathbb{R} \textit{ piecewise continuous})(\exists \tau \in \mathbb{R})$$
$$\Phi_T^{f+g\,u^1(t)}(q^0) = \Phi_\tau^g \circ \Phi_T^{f+g\,u^2(t)}(q^0).$$

Proof. Let $u^1, u^2 : \mathbb{R} \to \mathbb{R}$ be piecewise continuous. Since $[f, g] = 0$, $[f, g\,u^i(t)] = 0$ as well for $i = 1, 2$, which in turn implies that

$$\Phi_t^{f+g\,u^i(t)}(q^0) = \Phi_t^{g\,u^i(t)} \circ \Phi_t^f(q^0), \quad i = 1, 2.$$

Letting $q^1 := \Phi_t^f(q^0)$, we have

$$\Phi_t^{f+g\,u^i(t)}(q^0) = \Phi_t^{g\,u^i(t)}(q^1), \quad i = 1, 2.$$

Denoting $U^i(t) := \int_0^t u^i(\tau)d\tau$, we have

$$\Phi_t^{g\,u^i(t)}(q^1) = \Phi_{U^i(t)}^g(q^1), \quad i = 1, 2,$$

and thus

$$\Phi_t^{f+g\,u^1(t)}(q^0) = \Phi_{U^1(t)}^g(q^1) = \Phi_{U^1(t)-U^2(t)}^g \circ \Phi_{U^2(t)}^g(q^1)$$
$$= \Phi_{U_1(t)-U_2(t)}^g \circ \Phi_t^{f+g\,u^2(t)}(q^0).$$

Setting $\tau = U_1(t) - U_2(t)$ concludes the proof. □

REFERENCES

[1] T. McGeer, "Passive dynamic walking," *International Journal of Robotics Research*, vol. 9, no. 2, pp. 62–82, 1990.

[2] M. Garcia, A. Chatterjee, A. Ruina, and M. Coleman, "The Simplest Walking Model: Stability, Complexity, and Scaling," *Journal of Biomechanical Engineering*, vol. 120, no. 2, pp. 281–288, 04 1998.

[3] A. Goswami, B. Espiau, and A. Keramane, "Passive dynamic walking," *Autonomous Robots*, vol. 4, pp. 273–286, 1997.

[4] M. Spong and G. Bhatia, "Further results on control of the compass gait biped," in *Proceedings 2003 IEEE/RSJ International Conference on Intelligent Robots and Systems (IROS 2003) (Cat. No.03CH37453)*, vol. 2, 2003, pp. 1933–1938 vol.2.

[5] M. W. Spong, "Passivity based control of the compass gait biped," *IFAC Proceedings Volumes*, vol. 32, no. 2, pp. 506–510, 1999, 14th IFAC World Congress 1999, Beijing, China, 5-9 July.

[6] M. Spong and F. Bullo, "Controlled symmetries and passive walking," *IEEE Transactions on Automatic Control*, vol. 50, no. 7, pp. 1025–1031, 2005.

[7] F. Asano, M. Yamakita, N. Kamamichi, and Z.-W. Luo, "A novel gait generation for biped walking robots based on mechanical energy constraint," *IEEE Transactions on Robotics and Automation*, vol. 20, no. 3, pp. 565–573, 2004.

[8] J. Grizzle, G. Abba, and F. Plestan, "Asymptotically stable walking for biped robots: Analysis via systems with impulse effects," *IEEE Transactions on Automatic Control*, vol. 46, no. 1, pp. 51–64, January 2001.

[9] E. Westervelt, J. Grizzle, and D. Koditschek, "Hybrid zero dynamics of planar biped walkers," *IEEE Transactions on Automatic Control*, vol. 48, no. 1, pp. 42–56, January 2003.

[10] F. Plestan, J. Grizzle, E. Westervelt, and G. Abba, "Stable walking of a 7-dof biped robot," *IEEE Transactions on Robotics and Automation*, vol. 19, no. 4, pp. 653–668, August 2003.

[11] C. Chevallereau, G. Abba, Y. Aoustin, F. Plestan, E. Westervelt, C. C. de Wit, and J. Grizzle, "Rabbit: A testbed for advanced control theory," *IEEE Control Systems Magazine*, vol. 23, no. 5, pp. 57–79, October 2003.

[12] E. Westervelt, J. Grizzle, C. Chevallereau, J. Choi, and B. Morris, *Feedback Control of Dynamic Bipedal Robot Locomotion*. Florida, United States: CRC Press, 2007.

[13] E. Westervelt, B. Morris, and K. Farrell, "Analysis results and tools for the control of planar bipedal gaits using hybrid zero dynamics," *Autonomous Robots*, vol. 23, no. 2, p. 131–145, 2007.

[14] J. Grizzle, J. Hurst, B. Morris, H. Park, and K. Sreenath, "Mabel, a new robotic bipedal walker and runner," in *American Control Conference*, St. Louis, United States, June 2009, pp. 2030 – 2036.

[15] A. E. Martin, D. C. Post, and J. P. Schmiedeler, "Design and experimental implementation of a hybrid zero dynamics-based controller for planar bipeds with curved feet," *The International Journal of Robotics Research*, vol. 33, no. 7, pp. 988–1005, 2014.

[16] R. Sinnet, S. Jiang, and A. Ames, "A human-inspired framework for bipedal robotic walking design," *Int. J. of Biomechatronics and Biomedical Robotics*, vol. 3, pp. 20 – 41, 01 2014.

[17] A. Hereid, E. A. Cousineau, C. M. Hubicki, and A. D. Ames, "3d dynamic walking with underactuated humanoid robots: A direct collocation framework for optimizing hybrid zero dynamics," in *2016 IEEE International Conference on Robotics and Automation (ICRA)*, 2016, pp. 1447–1454.

[18] Y. Gong, R. Hartley, X. Da, A. Hereid, O. Harib, J.-K. Huang, and J. Grizzle, "Feedback control of a cassie bipedal robot: Walking, standing, and riding a segway," in *2019 American Control Conference (ACC)*, 2019, pp. 4559–4566.

[19] H. Zhao, J. Horn, J. Reher, V. Paredes, and A. D. Ames, "Multicontact locomotion on transfemoral prostheses via hybrid system models and optimization-based control," *IEEE Transactions on Automation Science and Engineering*, vol. 13, no. 2, pp. 502–513, 2016.

[20] R. Gregg, T. Lenzi, L. Hargrove, and J. Sensinger, "Virtual constraint control of a powered prosthetic leg: From simulation to experiments with transfemoral amputees," *IEEE Transactions on Robotics*, vol. 30, no. 6, pp. 1455–1471, 2014.

[21] O. Harib, A. Hereid, A. Agrawal, T. Gurriet, S. Finet, G. Boeris, A. Duburcq, M. E. Mungai, M. Masselin, A. D. Ames, K. Sreenath, and J. W. Grizzle, "Feedback control of an exoskeleton for paraplegics: Toward robustly stable, hands-free dynamic walking," *IEEE Control Systems Magazine*, vol. 38, no. 6, pp. 61–87, 2018.

[22] K. Hamed and J. Grizzle, "Reduced-order framework for exponential stabilization of periodic orbits on parameterized hybrid zero dynamics manifolds: Application to bipedal locomotion," *Nonlinear Analysis: Hybrid Systems*, vol. 25, pp. 227–245, August 2017.

[23] A. Hereid, C. M. Hubicki, E. A. Cousineau, and A. D. Ames, "Dynamic humanoid locomotion: A scalable formulation for hzd gait optimization," *IEEE Transactions on Robotics*, vol. 34, no. 2, pp. 370–387, 2018.

[24] A. Ramezani, J. W. Hurst, K. A. Hamed, and J. W. Grizzle, "Performance analysis and feedback control of atrias, a three-dimensional bipedal robot," *Journal of dynamic systems, measurement, and control*, vol. 136, no. 2, pp. 21 012–, 2014.

[25] R. Otsason and M. Maggiore, "On the generation of virtual holonomic constraints for mechanical systems with underactuation degree one," in *in 58th IEEE Conference on Decision and Control*, Nice, France, December 2019, pp. 8054–8060.

[26] J. Grizzle and C. Chevallereau, "Virtual constraints and hybrid zero dynamics for realizing underactuated bipedal locomotion," in *Humanoid Robotics: A Reference*, A. Goswami and P. Vadakkepat, Eds. Dordrecht, Netherlands: Springer Netherlands, 2019, pp. 1045–1075.

[27] N. Murakami, A. Sugimori, T. Ibuki, and M. Sampei, "Rolling motion control inducing back bending for acrobot composed of rounded links," in *20th IFAC World Congress*, Toulouse, France, July 2017, pp. 764–769.

[28] J. Nakanishi, T. Fukuda, and D. Koditschek, "A brachiating robot controller," *IEEE Transactions on Robotics and Automation*, vol. 16, no. 2, pp. 109–123, 2000.

[29] T. Fukuda and F. Saito, "Motion control of a brachiation robot," *Robotics and Autonomous Systems*, vol. 18, no. 1, pp. 83–93, 1996.

[30] M. W. Gomes and A. L. Ruina, "A five-link 2d brachiating ape model with life-like zero-energy-cost motions," *Journal of Theoretical Biology*, vol. 237, no. 3, pp. 265–278, 2005.

[31] F. Asano, "A novel generation method for underactuated bipedal gait with landing position control of swing leg based on property of zero dynamics," in *2015 IEEE International Conference on Advanced Intelligent Mechatronics (AIM)*, 2015, pp. 1184–1189.

[32] R. Goebel, R. Sanfelice, and A. Teel, *Hybrid Dynamical Systems: modeling, stability, and robustness*. Princeton University Press, 2012.

[33] M. Maggiore and L. Consolini, "Virtual holonomic constraints for Euler-Lagrange systems," *IEEE Transactions on Automatic Control*, vol. 58, no. 4, pp. 1001–1008, 2013.

[34] L. Consolini, A. Costalunga, and M. Maggiore, "A coordinate-free theory of virtual holonomic constraints," *Journal of Geometric Mechanics*, vol. 10, no. 4, pp. 467–502, 2018.

[35] A. Isidori, *Nonlinear Control Systems*, 3rd ed. Berlin, Germany: Springer-Verlag, 1995.

[36] A. Mohammadi, M. Maggiore, and L. Consolini, "On the Lagrangian structure of reduced dynamics under virtual holonomic constraints," *ESAIM: Control, Optimisation and Calculus of Variations*, vol. 23, no. 3, pp. 913–935, April 2017.

[37] E. Kao-Vukovich, "Virtual constraint generation for stable acrobot gaits," Master's thesis, University of Toronto, Toronto, 2020.

[38] L. Hunt, "n-dimensional controllability with $(n-1)$ controls," *IEEE Transactions on Automatic Control*, vol. 27, no. 1, pp. 113–117, 1982.

[39] M. Kelly, "An introduction to trajectory optimization: How to do your own direct collocation," *Society for Industrial and Applied Mathematics Review*, vol. 59, no. 4, pp. 849–904, 2017.

[40] A. Mohammadi, "Virtual holonomic constraints for euler-lagrange control systems," Ph.D. dissertation, University of Toronto (Canada), 2016.

[41] A. M. Kohl, E. Kelasidi, A. Mohammadi, M. Maggiore, and K. Y. Pettersen, "Planar maneuvering control of underwater snake robots using virtual holonomic constraints," *Bioinspiration & Biomimetics*, vol. 11, no. 6, p. 065005, 2016.

[42] A. Hereid and A. D. Ames, "Frost: Fast robot optimization and simulation toolkit," in *2017 IEEE/RSJ International Conference on Intelligent Robots and Systems (IROS)*, 2017, pp. 719–726.